

Modeling of Modular Multilevel Converters using Extended-Frequency Dynamics Phasors

By
Shailajah Rajesvaran

A thesis submitted to the Faculty of Graduate Studies of
The University of Manitoba
in partial fulfilment of the requirements for the degree of

MASTER OF SCIENCE

Department of Electrical and Computer Engineering
University of Manitoba
Winnipeg, Manitoba

August 2016

Copyright © 2016 by Shailajah Rajesvaran

Abstract

This thesis investigates modeling of modular multilevel converters (MMCs) using an averaging method known as extended-frequency dynamic phasors. An MMC can be used as an inverter or a rectifier in high voltage direct current (HVDC) system. This research develops a dynamic phasor model for an MMC operated as an inverter.

Extended-frequency dynamic phasors are used to model a system with only interested harmonics present. The developed model is capable of capturing both the low and high-frequency dynamic behavior of the converter depending on the requirements of the study to be performed.

The selected MMC model has 5 submodules per arm (6-level converter), nearest level control, capacitor voltage balancing, direct control and phase-locked loop (PLL) synchronization. With the above features, the developed dynamic phasor model is validated with electromagnetic transient model is developed using PSCAD simulation software.

The results are compared at transient and steady state with disturbances. The main computational advantage of this modeling is achieving less simulation time with inclusion of harmonics of interest.

Acknowledgments

First and foremost, I would like to thank my supervisor Prof. Shaahin Filizadeh for accepting me as his student and his valuable guidance throughout this research. I would also like to thank my examining committee, Prof. U.D. Annakkage and Prof. Mark Tachie, for their valuable time spent on my thesis and helpful comments.

So much thanks to Prof. A.M. Gole and Prof. A.D. Rajapakse for teaching me the courses, which are really useful for my research and carrier.

Special thanks to Prof. U.D. Annakkage for the help, advice and encouragement.

I also want to thank my family for sending me far away from my country and giving hope and positive strength to complete this work successfully. Thanks to my dear friends who helped me.

A special thanks to my husband, Mr. S. Arunprasanth, for his support, guidance and great ideas throughout this thesis work.

I would like to thank the Faculty of Graduate Studies and University of Manitoba staffs and technicians.

Finally I would like to thank the Natural Sciences and Engineering Research Council (NSERC) of Canada, MITACS Accelerate, and Manitoba Hydro for provide funding to this research.

Dedication

To my beloved mom, sisters, and my husband....

Contents

Front Matter

Contents	v
List of Tables.....	viii
List of Figures	ix
List of abbreviations	xii
List of Symbols.....	xiii
1 Introduction	1
1.1 Background	1
1.2 Problem definition	3
1.3 Thesis motivation	4
1.4 Thesis organization	5
2 Modular Multilevel Converters: Theory and Operation	7
2.1 Circuit topology of a conventional MMC	8
2.1.1 Half-bridge submodule: current paths and conduction.....	10
2.2 Switching techniques of submodules	12
2.2.1 Sinusoidal pulse-width modulation (SPWM).....	13
2.2.2 Nearest level control (NLC).....	15
2.2.3 Other switching techniques for MMCs	17
2.3 Capacitor voltage balancing	18
2.4 Converter control methodologies	19

2.4.1	Direct control.....	19
2.4.2	Decoupled control.....	21
2.5	Synchronization	23
2.6	Generating reference signals	24
2.7	Summary.....	25
3	Dynamic Phasors: Mathematical Preliminaries	26
3.1	Dynamic phasor principles.....	27
3.2	Dynamic phasor modeling applications.....	28
3.3	Dynamic phasor modeling of a converter system.....	29
3.3.1	Description of the converter circuit.....	30
3.3.2	Model validation	31
3.4	Summary.....	35
4	Dynamic Phasor Modeling of an MMC	36
4.1	State equations of an MMC.....	36
4.2	Dynamic phasor equations of MMC.....	39
4.3	Solving dynamic phasor equations	42
4.3.1	Selection of a numerical integration method.....	42
4.3.2	Trapezoidal method of integration.....	43
4.4	Summary.....	44
5	Dynamic Phasor Modeling of the Converter Control System	45
5.1	Modeling of power and voltage controllers	45
5.1.1	Real power controller.....	46
5.1.2	Terminal RMS voltage controller model.....	48
5.1.3	Nearest level control and voltage reference.....	51
5.2	Dynamic phasor modeling of PLL.....	51
5.3	Switching signal generation.....	52
5.4	Summary.....	54

6	Validation of the Dynamic Phasor Model of the MMC	55
6.1	MMC test system specifications.....	55
6.2	Electromagnetic transient simulation model.....	57
6.3	Comparison of simulation results.....	58
6.3.1	Simulation results at steady state.....	59
6.3.2	Simulation results for a step change in voltage reference.....	64
6.3.3	Results with a step change in power order.....	67
6.4	Analysis on the accuracy of the model.....	69
6.5	Summary.....	71
7	Contributions, Conclusions, and Future work	73
7.1	Contributions and conclusions.....	73
7.2	Future work.....	76
	Matter	78
	References.....	78

List of Tables

Table 2.1: Relationship between switching signals and the submodule output voltage.....	9
Table 2.2: Switching states for $N = 5$	11
Table 2.3: SPWM switching technique for 2-level converter.....	14
Table 3.1: Test system parameters.....	32
Table 6.1: MMC system parameters.....	56
Table 6.2: Controller parameters.....	57
Table 6.3: RMS voltage error for odd harmonic addition respective to Figure 6.2.....	70

List of Figures

Figure 2.1: Schematic diagram of an MMC with half-bridge submodules.	8
Figure 2.2: Types of submodules (a) half-bridge, (b) full-bridge.....	9
Figure 2.3: Half-bridge submodule output (a) V_{cap} and (b) 0.	10
Figure 2.4: Converter output voltage for a given switching state.....	11
Figure 2.5: A 2-level converter.....	13
Figure 2.6: PWM switching signal generation for a 2-level converter.....	14
Figure 2.7: The nearest level switching method.	15
Figure 2.8: Schematic diagram of a converter connected to an ac network.	19
Figure 2.9: Components of direct controller.....	20
Figure 2.10: Block diagram of decoupled control.	22
Figure 2.11: Block diagram of phase-locked loop.....	23
Figure 2.12: Reference signal generation.	24
Figure 3.1: Single-phase fully-controlled rectifier circuit.	30
Figure 3.2: Output current (top) and output voltage (bottom).....	32
Figure 3.3: Output current (top) and output voltage (bottom) with inclusion of harmonics.	33
Figure 3.4: Harmonic spectrum of output current (top) and output voltage (bottom) for firing angle change.....	34

Figure 4.1: Circuit diagram of an MMC.....	37
Figure 4.2: Half-bridge submodule circuit.....	37
Figure 5.1: Block diagram of the direct controller: (a) real power controller, (b) terminal voltage controller.	46
Figure 5.2: Block diagram of phasor model of PLL.....	52
Figure 6.1: Block diagram of the MMC system.	58
Figure 6.2: Progressive harmonic addition to the dynamic phasor model and comparison with the EMT.	60
Figure 6.3: (Top) Harmonic spectrum of the terminal voltage of 5-level converter (bottom) Zoomed version of the spectrum excluding the fundamental.....	61
Figure 6.4: Comparison of voltage (top) and current (bottom) at steady state fundamental only.	62
Figure 6.5: Comparison of voltage (top) and current (bottom) at steady state with harmonics.....	63
Figure 6.6: Comparison of voltage (top) and current (bottom) at the steady state with inclusion of harmonics up to 17 th in both models.....	64
Figure 6.7: Response to a step change in terminal voltage.....	65
Figure 6.8: Comparison of voltage (top) and current (bottom) fundamental only to a step change in the voltage reference.....	65
Figure 6.9: Comparison of voltage (top) and current (bottom) with harmonics to a step change in the voltage reference.....	66
Figure 6.10: Harmonic variation for the step change in terminal voltage.	67
Figure 6.11: Response to a step change in terminal real power.....	67

Figure 6.12: Comparison of voltage (top) and current (bottom) fundamental only to a step change in the power reference.	68
Figure 6.13: Comparison of voltage (top) and current (bottom) with harmonics to a step change in the power reference.	69
Figure 6.14: Comparison between voltage waveforms of EMT and dynamic phasor model	70
Figure 6.15: Comparison of the model error as a function of harmonics included.	71

List of abbreviations

AC – Alternative current

DC – Direct current

HVDC – High voltage direct current

LCC – Line commutated converter

VSC – Voltage-sourced converter

MMC – Modular multilevel converter

SM – Submodule

NLC – Nearest level control

PWM – Pulse with modulation

CVB – Capacitor voltage balancing

PLL – Phase-locked loop

PI – Proportional integral

PV – Power and voltage

DP – Dynamic phasor

IGBT – Insulated-gate bipolar transistors

RMS – Root mean square

FFT – Fast Fourier transform

EMT – Electromagnetic transient

List of Symbols

N – Number of submodules per arm

V_{dc} – DC link voltage

r – DC source internal resistance

i_{dc} – DC current

V_{cap} – Capacitor voltage

V_{SM} – Submodule voltage

L, L_{arm} – Arm inductance

R, R_{arm} – Arm resistance

V_t – Terminal voltage

V_s – Source voltage

L_s – AC network Thévenin inductance

R_s – AC network Thévenin resistance

L_{tf} – transformer inductance

C_m – Submodule capacitance

V_{conv} – Converter voltage

P – Real power

Q – Reactive power

X – Reactance

P_m – Measured power

P_{ref} – Reference power

V_m, V_{meas} – Measured voltage

V_o, V_{out} – Output voltage

V_{ref} – Reference voltage

m – Modulation index

δ – Phase angle

θ – PLL angle

u – Upper arm

l – Lower arm

d – Difference between upper and lower arm quantities

s – Sum of the upper and lower arm quantities

i – Current

V_{av} – Submodule average voltage

n – Switching functions

V_{av} – Submodule average voltage

V_c – Sum of submodule voltages

f – Frequency

ω – Angular frequency

λ – Phases (a, b, c)

j – Representation of imaginary part in complex numbers

k – Harmonic number

Chapter 1

Introduction

1.1 Background

Power systems rely increasingly on advanced power electronic converters for rapid control of real and reactive power and for long-distance power transmission. There are several converter technologies available for various applications in power systems including line-commutated converters (LCCs) and voltage-sourced converters (VSCs) such as conventional two-level, multilevel, and modular multilevel converters (MMCs).

An area of rapid growth wherein high-power electronic converters have played an enabling role is bulk power dc transmission. In high-voltage direct current (HVDC) transmission systems, thyristor-based line-commutated converters have been used for decades. LCC-HVDC offers the benefits of a mature technology and is available at ratings reaching thousands of MW per converter. LCC-HVDC systems, however, suffer from inherent technical challenges such as large filtering requirements, limited ability to operate into weak ac systems, and converter commutation failure [1]-[2].

As such a new breed of HVDC converters, which are based upon voltage-sourced converters and are commonly known as VSC-HVDC, have been pursued to alleviate these problems. A voltage-sourced converter is the most common type of self-commutated converter, which uses fully controlled semiconductor devices such as insulated-gate bipolar transistors (IGBTs) as switching devices [1]-[4]. These semiconductors have gained importance over the years and, due to their reliability, are most commonly used in such challenging applications as traction and industrial drives [1]-[2]. To reduce low-order harmonics, the number of levels in the output voltage of a VSC needs to be increased. Therefore, multilevel voltage-sourced converters were introduced, which use complicated arrays of controlled switches and multiple dc capacitors to create several voltage levels at the ac side [3]-[5].

Later a class of VSC topologies, known as modular multilevel converters, were introduced. This class of converters is based upon stacking a large number of identical units, known as submodules, to achieve a large number of output voltage levels so that an exceedingly accurate replica of a sinusoidal waveform can be achieved at the converter output [1]-[6]. The benefits of MMC-based HVDC converters are achieved at the expense of increased control and operating complexity. MMCs deploy a large number of submodule capacitors, whose voltages need to be tightly regulated and balanced for proper operation. Additionally, generation of high-quality output voltage waveforms without incurring large switching losses requires the use of advanced waveform synthesis techniques [1], [3]-[6].

The majority of MMC studies to date have relied on computer simulations. MMC models with reduced computational intensity fall into two general categories of average

(i.e., low frequency) models, and low-intensity full order (also known as detailed equivalent) models [7]. Low-order average-value models are inherently unable to capture transients of high frequency, and detailed models naturally include as many details as possible within the simulation bandwidth [7]-[8]. Generally, MMC models are developed with a pre-determined modeling outcome in mind.

This thesis proposes a new MMC model by using the concept of generalized state-space averaging [9], which in its most basic form reduces to what is normally known as dynamic phasors.

1.2 Problem definition

Dynamic phasors have already been used to model converters such as LCC-HVDC and VSC-HVDC and these models have been validated with the dominant harmonics (normally against the detailed switching-level electromagnetic transient simulation models) [10]-[12].

There is little work done in modeling of power systems including harmonics using dynamic phasors. Most of the work done using dynamic phasors has concentrated on the fundamental (and occasionally the first dominant harmonic), which completely ignores other harmonics [10], [13]-[17].

In MMC, output voltage contains considerable low order harmonics. The higher the levels in MMC results the lower the low order harmonics. Modeling of MMC using dynamic phasors is quite challengeable due its circuit complexity. Therefore most of the

dynamic phasor models of MMC consider only few low order harmonics (dc, fundamental and second harmonics).

This research, modeling of MMCs using extended-frequency dynamic phasors is based upon decomposing a (quasi-) periodic waveform into constituent harmonics, which can be included in the final model. The model contains details of the MMC's control system including its high-level control circuitry, as well as voltage balancing and synchronization components. The developed model is then validated by comparing it against a fully-detailed electromagnetic transient (EMT) simulation model developed in PSCAD/EMTDC simulator. Comparisons are made to establish the accuracy of the model (both its low-order and wide-band variants), and to assess the computational advantages it offers compared to conventional EMT models.

1.3 Thesis motivation

Extended-frequency dynamic phasors are able to decompose quasi-periodic waveforms into Fourier components and describe their time-domain dynamics. They are suitable for analyzing the fundamental and harmonic behavior of power electronic converter systems.

A preliminary (and only low-order) dynamic phasor model of an MMC system is presented in [15] and [16] wherein the eigenvalues of the system are studied; the presentations in [15] and [16], however, do not include any validation of the model. Another phasor model of an MMC is presented in [17], which is developed in a rotating reference frame. However, this model only includes the fundamental and the 2nd

harmonic corresponding to the MMC arm's circulating current. The above MMC models do not include arbitrary higher order harmonics.

From the model developed in this thesis, shorter simulation time will be achieved by considering only the harmonic components of interest. Individual harmonic-frequency models will allow development of screening mechanisms for harmonic interaction and stability studies. This model affords a high degree of control to the user to adjust the bandwidth of the model depending on the requirements of the study to be conducted. It is obvious to note that this modeling approach will also offer flexibility in its final computational complexity, as only the desired number of harmonics will be considered without having to model ones that are not required for the study at hand.

This research work will be of great value to the power systems industry in analyzing the dynamic behavior of converter-intensive systems in a rapid and computationally efficient manner.

1.4 Thesis organization

Chapter 2 presents a literature review on MMCs. This includes the circuit topology, controllers, and general operation of MMCs. Then, Chapter 3 presents dynamic phasor principles and applications, and a small example of dynamic phasor modeling of a single-phase fully controlled rectifier to familiarize the reader with this modeling approach. Chapter 4 explains how to apply dynamic phasors to modeling MMCs. Time-domain state-space equations and dynamic phasor equations for an MMC system are derived in Chapter 4, followed by dynamic phasor modeling of MMC controllers in Chapter 5. In

Chapter 5, dynamic phasor modeling of direct power and voltage controllers and phase-locked loops are discussed. For the validation of the developed dynamic phasor model, a well-known power system transient simulation tool, i.e., PSCAD/EMTDC, is selected. In Chapter 6, a brief introduction to PSCAD/EMTDC and the way it is used to model an MMC system are given. Dynamic phasor model validation and discussions are presented in this chapter by comparing the dynamic phasor model results with the results from the PSCAD/EMTDC simulation at steady state and during transients. Finally, Chapter 7 provides the conclusions and contributions of this thesis and also suggestions for future directions of research on this topic.

Chapter 2

Modular Multilevel Converters:

Theory and Operation

An MMC is an advanced voltage-source converter with multiple voltage levels at the output. It builds its multilevel output voltage using a cascaded connection of a large number of identical submodules. Provided that an adequately large number of submodules are available a smooth and nearly ideal sinusoidal waveform can be generated with an MMC, thereby significantly improving the harmonic contents of its output. Additionally, submodules can be switched at a significantly lower frequency than conventional two-level VSCs; therefore, an MMC offers improved harmonic performance and lower switching losses than two-level converters [1]-[3]. However, the operation of an MMC calls for additional control circuitry to ensure that submodule voltages are maintained and balanced; as a result of its complexity and also due to the large number of switching devices used in an MMC, modeling and simulation of an MMC is a challenging task.

2.1 Circuit topology of a conventional MMC

Figure 2.1 shows the circuit diagram of a conventional MMC. The output voltage is constructed by properly switching the submodules in the upper and lower arms. The sum of the submodule voltages produces a staircase output waveform. Commonly, half-bridge or full-bridge submodules are used in MMCs; the MMC shown in Figure 2.1 employs half-bridge submodules. Figure 2.2 shows the circuit diagram of the commonly used submodule types.

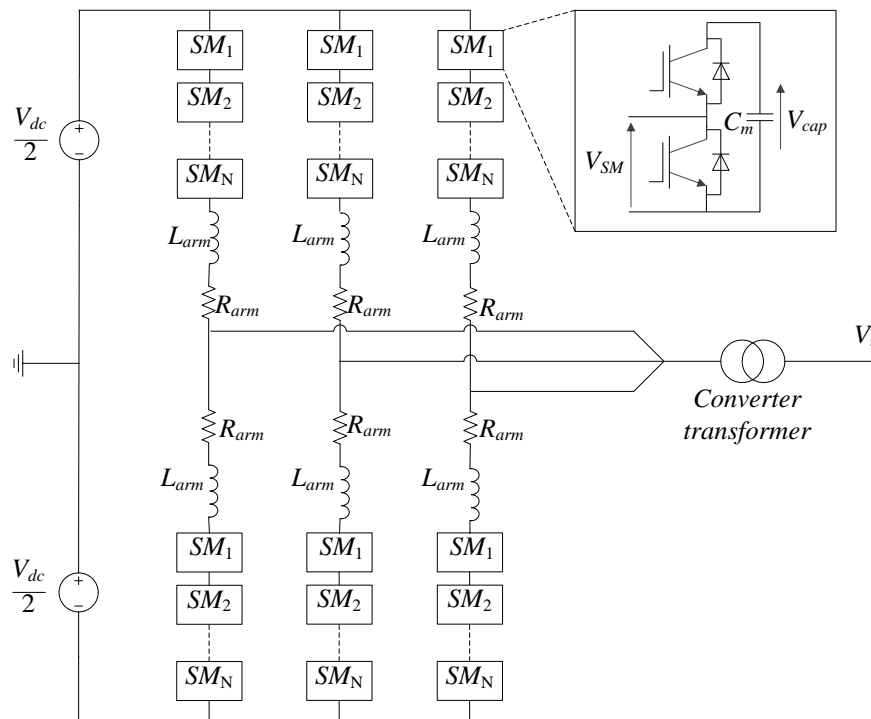


Figure 2.1: Schematic diagram of an MMC with half-bridge submodules.

The MMC in Figure 2.1 is grounded at the midpoint on the dc side and has an upper-arm and a lower-arm, which contain the submodules. For a three phase MMC, there will be 6 arms.

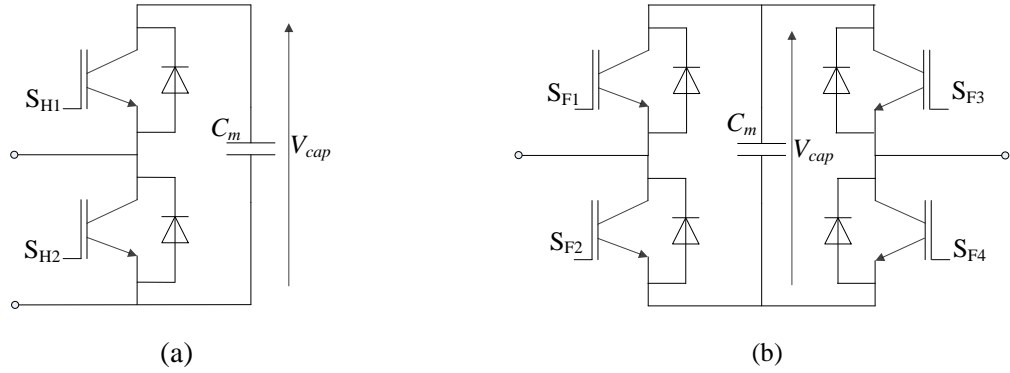


Figure 2.2: Types of submodules (a) half-bridge, (b) full-bridge.

A half-bridge submodule output voltage can be switched to either zero or its capacitor voltage, V_{cap} ; a full-bridge module can be switched to zero or $\pm V_{cap}$. The output of the submodule voltage is generated based on the switching signals given to the controlled switches. Table 2.1 shows the submodule output voltage and the corresponding switching signals.

Table 2.1: Relationship between switching signals and the submodule output voltage

Half-bridge submodule			Full-bridge submodule				
S_{H1}	S_{H2}	Output voltage	S_{F1}	S_{F2}	S_{F3}	S_{F4}	Output voltage
ON	OFF	V_{cap}	ON	OFF	OFF	ON	V_{cap}
OFF	ON	0	ON	OFF	ON	OFF	0
			OFF	ON	ON	OFF	$-V_{cap}$
			OFF	ON	OFF	ON	0

For the half-bridge submodule, complementary gate signals will be given to S_{H1} and S_{H2} to avoid short circuits across the submodule capacitor. Similarly, gate pulses to S_{F1} and S_{F2} and also S_{F3} and S_{F4} in a full-bridge submodule will be complementary.

2.1.1 Half-bridge submodule: current paths and conduction

Figure 2.3 shows the current paths for the two states (0 and V_{cap}) of a half-bridge submodule.

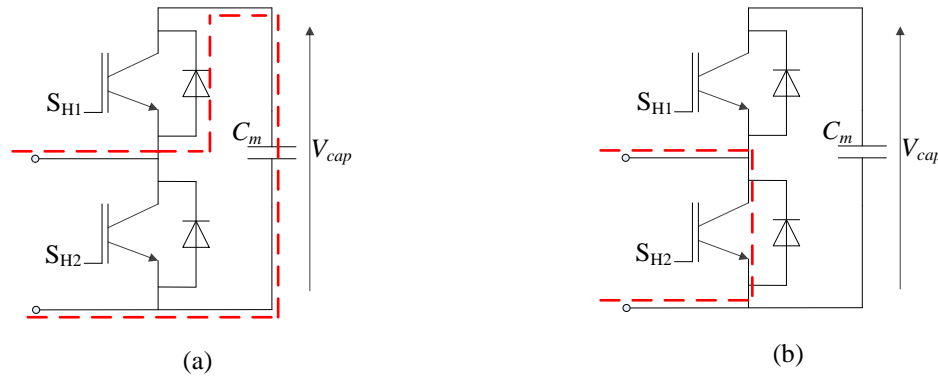


Figure 2.3: Half-bridge submodule output (a) V_{cap} and (b) 0.

The submodule capacitor voltage needs to be regulated to the nominal capacitor voltage value shown in (2.1).

$$V_{cap} = \frac{V_{dc}}{N} \quad (2.1)$$

To generate a sinusoidal voltage waveform, at any instant of time the total number of submodules that need to be turned on for a phase is equal to N . The number of levels in the converter output voltage depends on the number of submodules. If there are N submodules per arm, there will be $N+1$ levels in the converter's output voltage. For example, if $N=5$ is assumed the corresponding number of switches in the upper and lower arms will be as shown in Table 2.2.

Table 2.2: Switching states for $N = 5$.

Number of submodules to be turned on		Output voltage
Upper-arm	Lower-arm	
0	5	$\frac{V_{dc}}{2}$
1	4	$\frac{3V_{dc}}{10}$
2	3	$\frac{V_{dc}}{10}$
3	2	$-\frac{V_{dc}}{10}$
4	1	$-\frac{3V_{dc}}{10}$
5	0	$-\frac{V_{dc}}{2}$

An example of a switching state and the corresponding output voltage is shown in Figure 2.4.

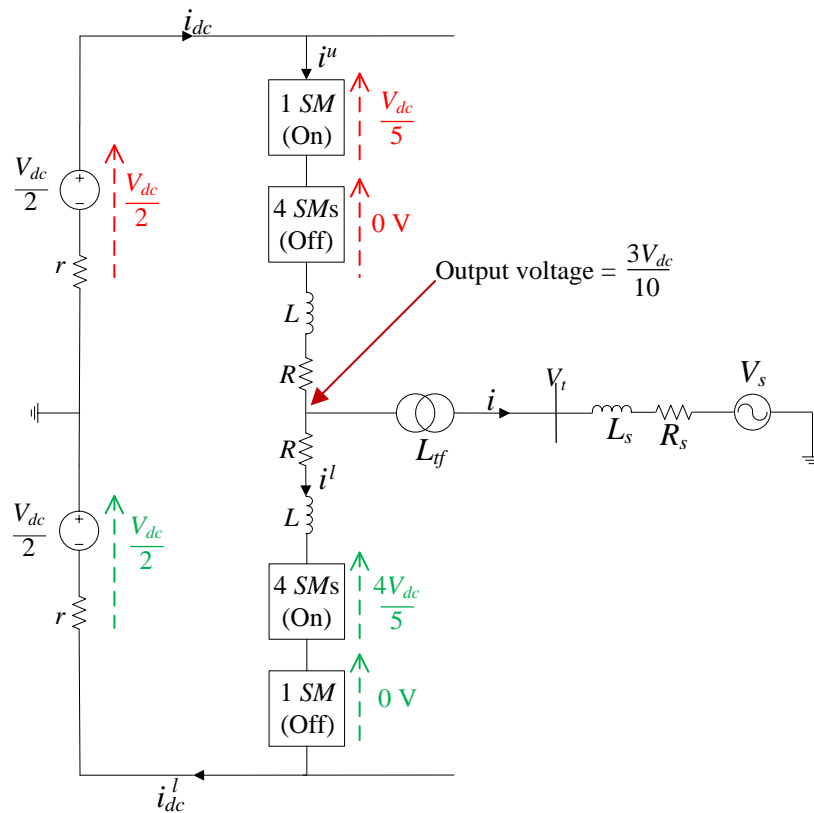


Figure 2.4: Converter output voltage for a given switching state

Figure 2.4 shows the converter output voltage when 1 submodule in the upper arm and 4 submodules in the lower arm are turned on.

Table 2.2, it must be noted that the peak value of the output voltage is $\frac{V_{dc}}{2}$ and the sum of the upper-arm and lower-arm submodules turned on is 5 ($=N$). Once the reference signal is generated, there are several switching techniques available to generate the switching signals for IGBTs. The reference signal is generated by using control system and it is explained in Section 2.6.

2.2 Switching techniques of submodules

There are several switching techniques available to turn on/off the submodules of a modular multilevel converter. Pulse-width modulation (PWM) is a popular, well-known modulation technique used in DC-AC converters. PWM methods can be classified into two categories of carrier-based phase shifted modulation and direct modulation with active selection methods [18]. Both methods are based on a high-frequency carrier signal; therefore, high-frequency switching leads to high switching losses in above converters.

There are several sub-categories of PWM, namely sinusoidal PWM (SPWM), harmonic injection PWM, optimal PWM (OPWM or selective harmonic elimination (SHE)) and space vector modulation (SVM), which can be used in MMCs [19]-[29].

Apart from PWM techniques, low-frequency switching techniques are also used to turn on/off MMC submodules. The nearest level control is one of the popular low-frequency switching methods. In this method, high-frequency carrier signals are not used. Therefore, it results in lower operational losses compared to the losses caused by PWM

techniques [30]. The down-side of nearest level control is that it requires a large number of submodules to attain an acceptable level of harmonic reduction.

2.2.1 Sinusoidal pulse-width modulation (SPWM)

The switches in the converter can be turned on and off as required. A simple way of switching is to turn on and off a switch only once in every cycle. However, if the same switch is turned on several times in a cycle, an improved harmonic profile may be achieved. Sinusoidal PWM (SPWM) is commonly used as a switching technique for VSCs and MMCs. In sinusoidal PWM, the generation of the desired output voltage is achieved by comparing the desired reference waveform (also called the modulating sinusoidal signal) with a high-frequency carrier wave (triangular wave). Circuit diagram of a two level VSC is shown in Figure 2.5 and Figure 2.6 shows the SPWM technique used for the VSC.

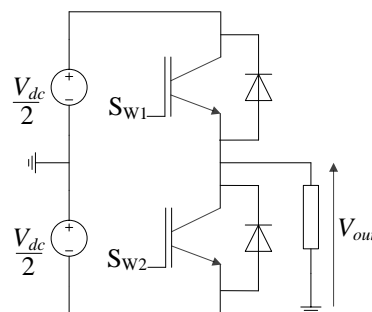


Figure 2.5: A 2-level converter.

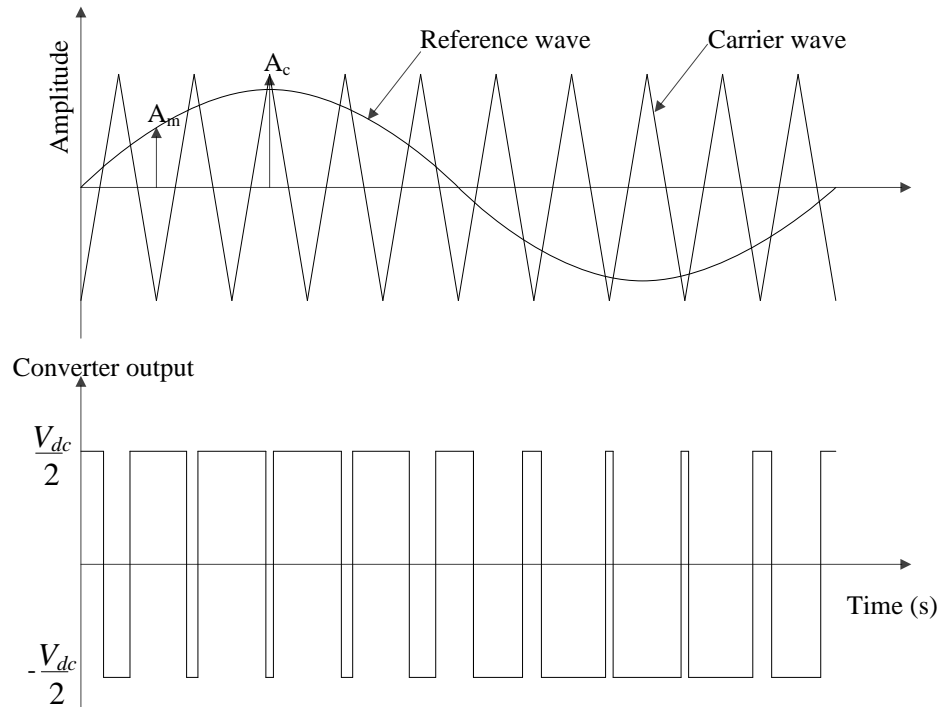


Figure 2.6: PWM switching signal generation for a 2-level converter.

When the reference waveform is greater than the carrier waveform then the top switch (S_{w1}) will be turned on and when the reference waveform is less than the carrier waveform the bottom switch will be turned on.

Table 2.3: SPWM switching technique for 2-level converter.

S_{w1}	S_{w2}	Output voltage
ON	OFF	$\frac{V_{dc}}{2}$
OFF	ON	$-\frac{V_{dc}}{2}$

If the modulating signal is sinusoidal with an amplitude A_m , and the amplitude of the triangular carrier signal is A_c , the ratio $m=A_m/A_c$ is known as the modulation index. The

amplitude of the applied output voltage is controlled by controlling the modulation index

(m); it can be shown that the amplitude of the output voltage V_o , is equal to $m \frac{V_{dc}}{2}$ [20].

For a modular multilevel converter, switching signals to each module are developed using different carrier waveforms. Phase-shifted carrier pulse-width modulation (PSC-PWM) and phase-disposition (PD) sinusoidal pulse-width modulation (PD-SPWM) for modular multilevel converter are explained in [20] and [21]. Typically switching frequencies in 2-15 kHz range are considered adequate for power systems applications. However, a higher carrier frequency does result in a larger number of switching per cycle and hence in increased switching losses [22].

2.2.2 Nearest level control (NLC)

NLC is a modulation techniques used to switch the submodules of an MMC at a low switching frequency. According to the total number of capacitors the nominal value of each capacitor will be decided and the output voltage will be constructed by a staircase of steps (of the nominal value) as shown in Figure 2.7.

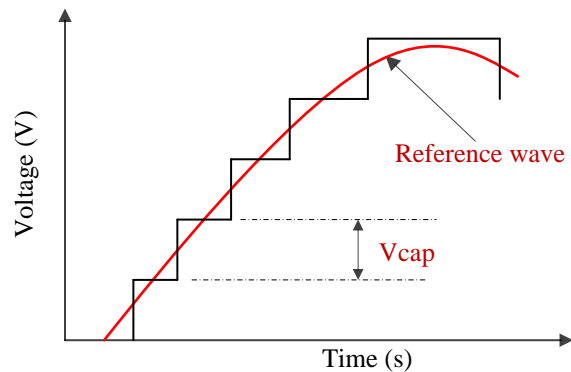


Figure 2.7: The nearest level switching method.

Firstly, the submodule capacitor voltage is calculated by dividing the DC voltage by the number of capacitors per arm (N). Then the staircase waveform is generated by comparing the reference wave with each step of the nominal capacitor voltage midpoint value as shown in (2.2).

For even values of N ,

$$V_{out} = \begin{cases} nV_{cap} & ; V_{ref} < \left(n + \frac{1}{2}\right)V_{cap} \\ (n+1)V_{cap} & ; V_{ref} > \left(n + \frac{1}{2}\right)V_{cap} \end{cases}$$

where $0 \leq n \leq \left(\frac{N}{2}\right)$

For odd values of N ,

$$V_{out} = \begin{cases} \left(n - \frac{1}{2}\right)V_{cap} & ; V_{ref} < nV_{cap} \\ \left(n + \frac{1}{2}\right)V_{cap} & ; V_{ref} > nV_{cap} \end{cases}$$

where $0 \leq n \leq \left(\frac{N-1}{2}\right)$ (2.2)

For the odd and even number of submodules per arm, the staircase waveform is different.

However, the final number of levels in the output staircase waveform is always $N+1$.

The staircase output waveform can be constructed by accommodating any kinds of changes (amplitude, phase, and frequency) in the reference waveform and it will follow the reference waveform in steady state and during transients. Also high-frequency switching as in PWM is not suitable for larger number of submodules; because larger no of switches cause high switching loss. Due to its low switching frequency and simplicity,

the nearest level control is considered as a suitable switching technique for MMCs with an adequately large number of submodules [30]. NLC is optimal from the RMS error standpoint, which is proved in Chapter 6.

2.2.3 Other switching techniques for MMCs

There are direct modulation methods, used in MMC submodule switching. Optimal PWM (OPWM), selective harmonic elimination, is used to eliminate a selected number of harmonics with the smallest number of switching. If there are n chops per quarter cycle, it will allow n degrees of freedom. Therefore, one can use these to eliminate $n-1$ harmonics while controlling the magnitude of the fundamental. This method, however, can be difficult to implement on-line due to computational and memory requirements and not suitable for larger number of submodules [23]-[25].

Another method for switching used in MMCs is space-vector modulation (SVM). It treats the converter as a single unit that can assume a finite number of states depending on the arrangement of the switches. According to the proper state combination, the switches will be turned on. The reference signal that is considered in this scheme is a rotating vector. This is suitable for lower level converters such as 2-level; as the number of states is less (8 states). Higher number of modules results in a larger number of states, and the implementation will become complex. Therefore, it is not a suitable method for multilevel converters [26]-[29].

2.3 Capacitor voltage balancing

In MMCs, each arm consists of a number of submodules and each submodule consists of a capacitor to produce an output voltage according to the switching pattern. The direction of the arm current influences each capacitor by either charging or discharging it. Therefore, a control algorithm is needed to regulate the voltage across each capacitor to its nominal level.

Although from the nearest level control or other PWM methods, the number of capacitors needs to be switched on at a time is known, one does not know which capacitors are to be switched on. To find that information, one needs to consider which capacitors to insert depending on the present values of the capacitor voltages and the direction of the phase current (charging or discharging). A simple sorting algorithm such as bubble sort can be used to produce a sorted list of present capacitor voltages. Bubble sort is a simple and effective sorting technique for larger number of data-points and is hence selected in this research.

This capacitor voltage balancing algorithm instructs that when the arm current is in the charging direction, the capacitors with the lowest voltages are to be turned on and when the current is in the discharging direction, the capacitors with the highest voltage are to be turned on [15], [30].

From the nearest level control, a staircase waveform will be resulted for the corresponding reference signal. For both the upper and the lower arms, arm current signals are used with the sorting algorithm to find the number of capacitors and which capacitors need to be turned on and off.

2.4 Converter control methodologies

In a converter, power flow can be controlled by controlling the modulation index and the phase angle of the reference voltage signal. Two types of control methods that are widely used in MMCs are the direct control and the decoupled control, as explained next.

2.4.1 Direct control

Direct control is the simplest way of controlling the power flow through a converter. The principle can be explained using the simple network shown in Figure 2.8. The converter is connected to an AC network through a reactor, which may represent the leakage reactance of the interfacing converter transformer.

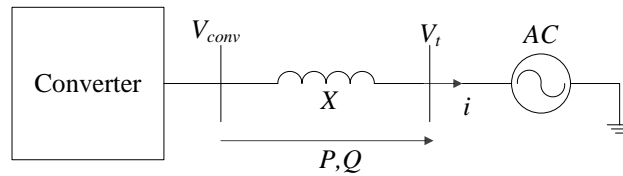


Figure 2.8: Schematic diagram of a converter connected to an ac network.

The general power flow equations are given in (2.3).

$$P = \frac{V_t \cdot V_{conv} \sin(\delta)}{X}$$

$$Q = \frac{V_t \cdot V_{conv} \cos(\delta) - V_t^2}{X} \quad (2.3)$$

δ is the angle between the converter voltage and terminal voltage. Normally, the phase angle, δ , is small. Therefore, the approximations $\sin \delta \approx \delta$ and $\cos \delta \approx 1$ can be applied to (2.3) and simplified equations shown in (2.4) are obtained.

$$P = \frac{V_t \cdot V_{conv} \cdot \delta}{X}$$

$$Q = \frac{V_t \cdot V_{conv} - V_t^2}{X} \quad (2.4)$$

The reactance X is a constant. The purpose is to control the terminal voltage and real power. By changing δ , the real power (P) is controlled to the desired value and by controlling the modulation index (m), the reactive power (Q) or terminal voltage (V_t) can be controlled [22]. The modulation index can be expressed as in (2.5),

$$m = \frac{(V_{conv})_{peak}}{V_{dc}/2} \quad (2.5)$$

The control of real power and terminal ac voltage are done using Proportional Integral (PI) controllers as shown in Figure 2.9.

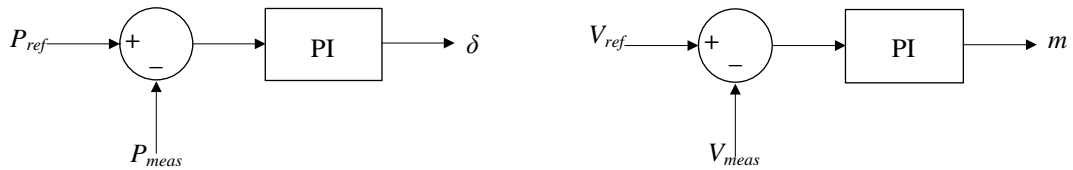


Figure 2.9: Components of direct controller.

The problem with the direct control method is that the change in δ affects the terminal AC voltage. In addition, the change in m affects the regulation of real power. In other words, changes in the variable will impact the other one causing undesirable interactions.

2.4.2 Decoupled control

To avoid cross-coupling of variables, the decoupled control method is introduced [31]-[32]. In this method, the parameters in the 3-phase domain (abc) are converted to the dq0 domain using Park's transformation as given in (2.6).

$$\begin{bmatrix} x_d \\ x_q \\ x_0 \end{bmatrix} = \frac{2}{3} \begin{bmatrix} \cos(\theta) & \cos\left(\theta - \frac{2\pi}{3}\right) & \cos\left(\theta + \frac{2\pi}{3}\right) \\ \sin(\theta) & \sin\left(\theta - \frac{2\pi}{3}\right) & \sin\left(\theta + \frac{2\pi}{3}\right) \\ \frac{1}{2} & \frac{1}{2} & \frac{1}{2} \end{bmatrix} \begin{bmatrix} x_a \\ x_b \\ x_c \end{bmatrix}$$

$$x_{dq0} = T \cdot x_{abc} \quad (2.6)$$

The measured real power and reactive power can be calculated using 3 phase voltages and currents as below.

$$P_m = V_{ta}i_a + V_{tb}i_b + V_{tc}i_c$$

$$Q_m = V_{tb}i_a + V_{tc}i_b + V_{ta}i_c \quad (2.7)$$

From Figure 2.8, the following equation (2.8) can be obtained.

$$(V_{conv})_{abc} = (V_t)_{abc} + L \frac{di_{abc}}{dt} \quad (2.8)$$

By using the parks transformation, equations (2.7) and (2.8) can be modified as below,

$$i_{dq0} = T i_{abc} \quad \text{and} \quad V_{tdq0} = T V_{tabc}$$

$$P_m = \frac{3}{2} V_{td} i_d + \frac{3}{2} V_{tq} i_q + V_{t0} i_0 \quad \text{and} \quad Q_m = \frac{3}{2} V_{td} i_q - \frac{3}{2} V_{tq} i_d$$

$$(V_{conv})_{dq0} = (V_t)_{dq0} + LT \frac{d(T^{-1}i_{dq0})}{dt}$$

$$(V_{conv})_{dq0} = (V_t)_{dq0} + L \frac{di_{dq0}}{dt} + L\omega \begin{bmatrix} 0 & 1 & 0 \\ -1 & 0 & 0 \\ 0 & 0 & 0 \end{bmatrix} i_{dq0} \quad (2.9)$$

Considering a balanced 3-phase system, the zero sequence can be neglected. The decoupled controller for (2.9) is shown in Figure 2.10.

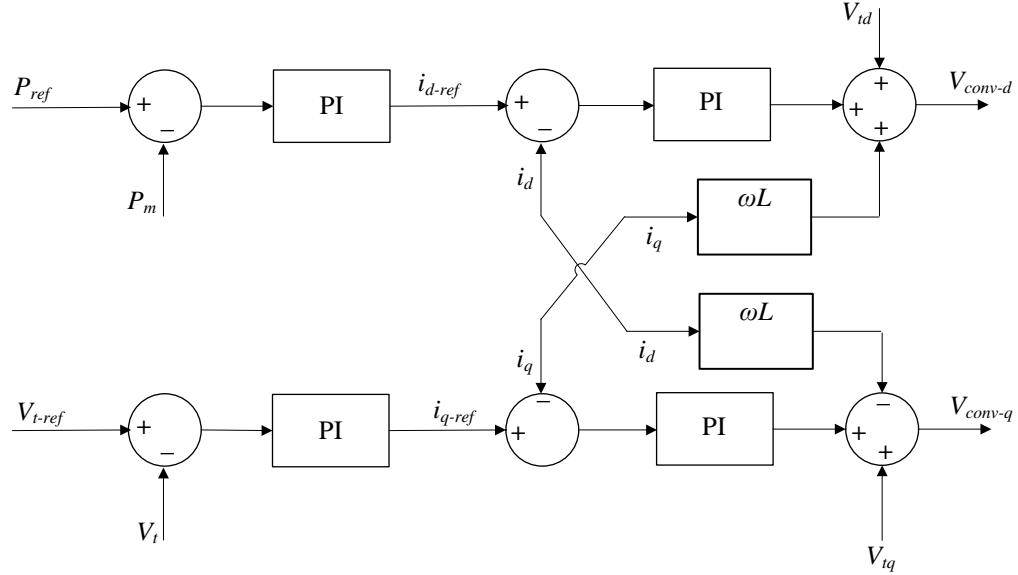


Figure 2.10: Block diagram of decoupled control.

The modulation index m and the phase angle δ can be found using the equations given in (2.10),

$$m = \frac{\sqrt{(V_{conv-d})^2 + (V_{conv-q})^2}}{V_{dc}}$$

$$\delta = \tan^{-1} \left(\frac{V_{conv-d}}{V_{conv-q}} \right) \quad (2.10)$$

By controlling m and δ , P_m and V_t can be controlled [31]-[32]. This control method consists of four PI-controllers and they need to be tuned. Therefore, this method is more complicated compared to the direct method.

2.5 Synchronization

To generate the reference signal for switching the submodules, a suitable synchronizing technique is required. Normally, the reference angle is measured with respect to the phase angle of the terminal ac voltage. To measure the phase angle, a suitable phase-locked loop (PLL) is used. There are several types of PLL architectures available in literature. The block diagram of a synchronous reference frame PLL [33] is shown in Figure 2.11.

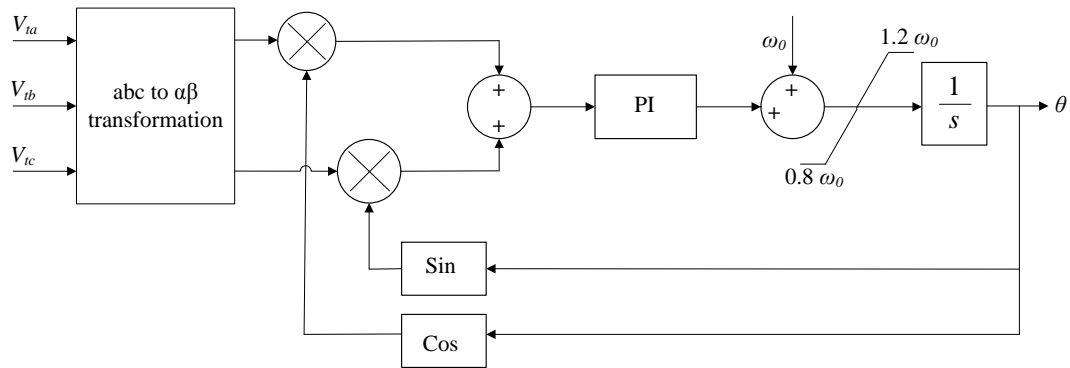


Figure 2.11: Block diagram of phase-locked loop.

Figure 2.11 shows the internal operation of PLL that was used to derive a reference phase angle (θ) of the terminal voltage. Three-phase terminal voltages (V_{ta} , V_{tb} , V_{tc}) are transformed to two phases ($V_{t\alpha}$, $V_{t\beta}$) by using abc to $\alpha\beta$ transformation. An error signal is calculated by using the PLL output angle (θ) and the voltages ($V_{t\alpha}$, $V_{t\beta}$) as shown in

Figure 2.11. The error is sent through a PI-controller and then through a resettable integrator to produce the angle θ . A fixed value (ω_0) controls the nominal tracking frequency of the PLL. If there is a phase error, the error signal is integrated through the PI controller and added to the system frequency. The aim of the PLL is to make the error equal to zero and make the PLL output angle equal to the terminal voltage vector angle. Therefore, the PLL always tracks the terminal voltage vector's angle for any phase error introduced by the external disturbances to the terminal voltage.

2.6 Generating reference signals

The terminal where all the measurements are taken and the voltage needs to be controlled is called the point of common coupling (PCC). From the direct or decoupled controlling techniques, the modulation index (m) and the phase angle (δ) can be obtained with respect to the terminal voltage and real power. In addition, the terminal voltage angle θ (with respect to the system connected to the terminal point) at the PCC can be found from the PLL. With the above values, the reference signals are generated for upper-arm and lower-arm separately as shown in Figure 2.12.

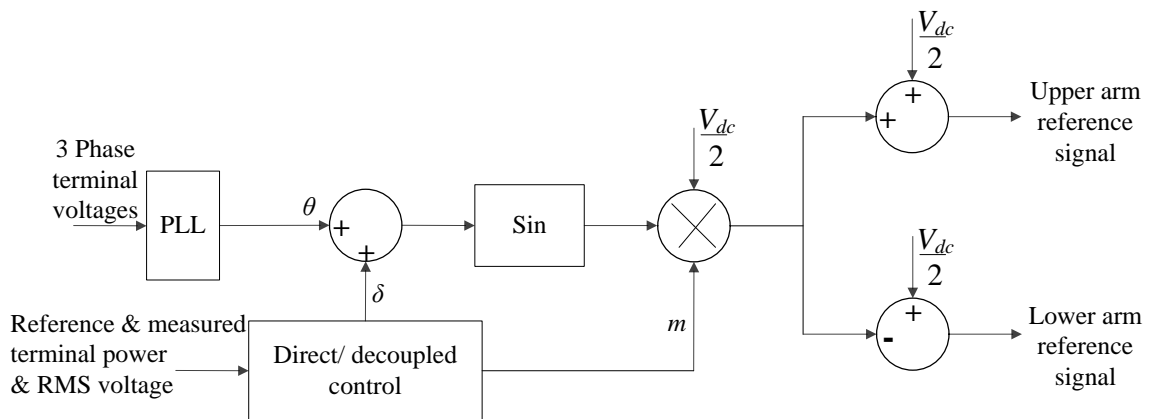


Figure 2.12: Reference signal generation.

At every instant the m , δ , and θ will be calculated and given as inputs to the reference signal; therefore, any system disturbances can be identified and regulated to the desired value.

2.7 Summary

In this chapter, the MMC topology, submodule types, and their operation were discussed. Different types of switching techniques used in converters to switch the modules and the merits and disadvantages of each method were discussed. Nearest Level control which used in this thesis was explained and a method to perform capacitor voltage balancing was also presented. The function of a phase-locked loop and its contribution to the MMC control was explained. Two common VSC control techniques were explained in detail using block diagrams. Finally the procedure of creating reference signals for the upper and lower arms of the MMC was explained.

Chapter 3

Dynamic Phasors: Mathematical

Preliminaries

Dynamic phasor modeling is used to represent the low frequency transients of a power system without considering high frequency components. Examination reveals that the Fourier coefficients obtained from generalized state space averaging are indeed dynamic phasors [9]. It decomposes voltage and current waveforms into harmonics and simply represents them in the form of Fourier coefficients [11]. Harmonics are produced by switching devices such as power electronic converters and nonlinear elements such as saturated core of a transformer. The magnitude and phase information of the Fourier coefficients for each harmonic can be represented as real and imaginary components as well.

Dynamic phasor-based models are useful to study a system's behaviour with inclusion of a number of harmonics (typically low-frequency ones). In addition, they allow the user to decide what level of detail to include in the model. Moreover, the

behaviour of each harmonic can be studied at steady state and during transients without simulating the complete harmonic spectrum of the system. Dynamic phasors are used to model synchronous generators, wind energy systems, and HVDC transmission systems [10-14].

3.1 Dynamic phasor principles

Generally, dynamic phasors are used to decompose waveforms into harmonics using Fourier coefficients. In mathematical terms, a Fourier series is a means to represent a periodic function as the sum of sines and cosines whose frequencies are integer multiple of the frequency of the original waveform. The Fourier series of a periodic signal over its period T_0 is given in (3.1) and the Fourier coefficients are given in (3.2)

$$x(\tau) = \sum_{k=-\infty}^{+\infty} \langle x \rangle_k(t) e^{j\omega k \tau} \quad \text{where, } \tau \in [t - T_0, t] \quad (3.1)$$

$$\langle x \rangle_k(t) = \frac{1}{T_0} \int_{t-T_0}^t x(\tau) e^{-j\omega k \tau} d\tau \quad (3.2)$$

For every value of k , the k^{th} harmonic coefficient of the function $x(t)$ can be found, which is the dynamic phasor representation of $x(t)$ for the k^{th} harmonic. The dynamic phasor of the derivative of a signal $x(t)$ can be obtained as given in (3.3).

$$\frac{d\langle x \rangle_k(t)}{dt} = \left\langle \frac{dx(t)}{dt} \right\rangle_k - j\omega k \langle x \rangle_k(t) \quad (3.3)$$

The dynamic phasor of the product of two signals $u(t)$ and $v(t)$ can be obtained by discrete convolution of the corresponding dynamic phasors as shown in (3.4).

$$\langle u(t)v(t) \rangle_k = \sum_{l=-\infty}^{+\infty} \langle u(t) \rangle_l \langle v(t) \rangle_{k-l} \quad (3.4)$$

$$\langle x(t) \rangle_{-k} = \langle x(t) \rangle_k^* \quad (3.5)$$

From (3.5), the conjugate of $x(t)$ can be found. Equations (3.2), (3.3), and (3.4) are often adequate to model a dynamical system in dynamic phasor domain. Then, (3.1) is used to convert the phasor-domain equations to time-domain equivalents. The time-domain model is developed to generate time-domain responses [9]-[15].

3.2 Dynamic phasor modeling applications

Dynamic phasor modeling has been used to model complex systems such as voltage-sourced converter HVDC (VSC-HVDC) system [10], line-commutated converter HVDC (LCC-HVDC) system models [11]-[12], electrical machines and wind generators [13]-[14], dc-dc converters [34], flexible ac transmission systems (FACTS) devices [35]-[36], and to study faults and dynamics of power systems [37]-[38].

MMC modeling using dynamic phasors has often been limited to the fundamental and the second harmonic in existing technical publications [15]-[17]; additionally a comprehensive validation of the developed models has not been presented in [15]-[16].

For a dynamical system, dynamic phasor equations can be written in two different ways. One method is directly through the Kirchhoff's voltage and current laws (KVL and

KCL) of the system and obtaining state equations to which dynamic phasor operators can be applied. The other way is converting the system to injecting current sources and conductance as it is done in many EMT simulation programs [39]. Both methods are used in previous works reported in literature.

In this research, state space analysis method is selected for dynamic phasor modeling of an MMC as it is simple and straightforward. An MMC model with direct real power-voltage control with inclusion of arbitrary harmonics is developed using dynamic phasors in the abc frame and the results are then validated against a fully detailed EMT model.

3.3 Dynamic phasor modeling of a converter system

This section shows a small example of dynamic phasor modeling of a simple single-phase fully-controlled rectifier. The circuit diagram of a controlled rectifier is shown in Figure 3.1. Validation of the DP model is done via comparisons with a detailed EMT of the converter implemented in the PSCAD/EMTDC electromagnetic transient simulator. The purpose of this example to demonstrate the modeling method on a switching converter with moderate complexity before it is applied to a complex MMC system.

3.3.1 Description of the converter circuit

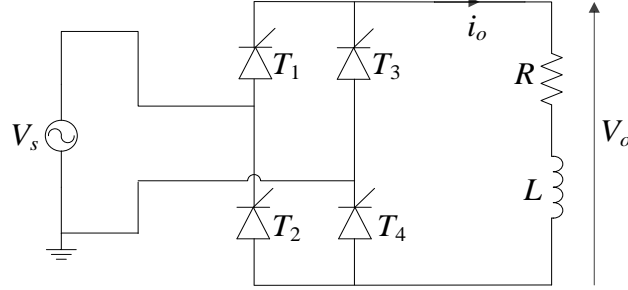


Figure 3.1: Single-phase fully-controlled rectifier circuit.

The considered fully-controlled rectifier has four thyristors denoted as T_1 , T_2 , T_3 , and T_4 . In the positive half cycle of the source voltage, $V_s(t)$, T_1 and T_4 are forward biased and will receive gate pulses and in the negative half cycle T_3 and T_2 will be forward biased and will receive gate pulses. (3.6) describes the dynamics of the output loop of the circuit.

$$\frac{di_o}{dt} = -\frac{R}{L}i_o + \frac{V_o}{L} \quad (3.6)$$

Dynamic phasor operators are applied to the state equation shown in (3.6). The resultant dynamic phasor equation is given in (3.7).

$$\left\langle \frac{di_o}{dt} \right\rangle_k = -\frac{R}{L}\langle i_o \rangle_k + \frac{\langle V_o \rangle_k}{L}$$

$$\frac{d\langle i_o \rangle_k}{dt} = -j\omega k \langle i_o \rangle_k - \frac{R}{L}\langle i_o \rangle_k + \frac{\langle V_s U \rangle_k}{L} \quad (3.7)$$

where, U is a switching function and it is a mathematical relationship that connects the input and output together. For each value of k , the corresponding harmonic model can be

found. This circuit is a rectifier; therefore, its output only consists of dc ($k = 0$) and even-numbered harmonics. For $k=0$, the dc part of the output current can be found and for $k=2, 4, 6, \dots$ the real and imaginary parts of each even harmonic component can be found. The resulting time-domain equations are shown in (3.8).

$$\begin{aligned}
 i_o(t) &= \langle i_o \rangle_0 + \langle i_o \rangle_2 e^{j2\omega_0(t-T_0)} + \langle i_o \rangle_{-2} e^{-j2\omega_0(t-T_0)} + \dots \\
 i_o(t) &= \langle i_o \rangle_0 + \sum_{k=2(\text{even})}^{\infty} \langle i_o \rangle_k e^{jk\omega_0(t-T_0)} + \langle i_o \rangle_{-k} e^{-jk\omega_0(t-T_0)} \\
 i_o(t) &\approx \langle i_o \rangle_0 + \sum_{k=2(\text{even})}^{\infty} \langle i_o \rangle_k e^{jk\omega_0(t-T_0)} + \langle i_o \rangle_k^* e^{-jk\omega_0(t-T_0)} \tag{3.8}
 \end{aligned}$$

In the output current, any number of harmonics can be included or one can only include a small number of constituent harmonic for a low-order model. Extended frequency dynamic phasor model of the single phase fully controlled rectifier is developed with the voltage source and RL load.

3.3.2 Model validation

A model of this converter circuit as shown in Figure 3.1 is developed in PSCAD/EMTDC transient simulator and the results are compared with those generated by the dynamic phasor model developed in MATLAB. The output current and voltage waveforms are observed, and for both models the same disturbance is applied by changing the value of the firing angle. The single phase fully controlled rectifier system parameters are given in Table 3.1.

Table 3.1: Test system parameters

Parameter	Value
AC source voltage (RMS)	120 V
Frequency	50 Hz
Resistance (R)	20 Ω
Inductance (L)	0.1 H

The thyristor firing angle (α) is selected as 45° . Then, at 0.5 s the firing angle is changed to 10° . The steady state and transient responses are shown in Figure 3.2.

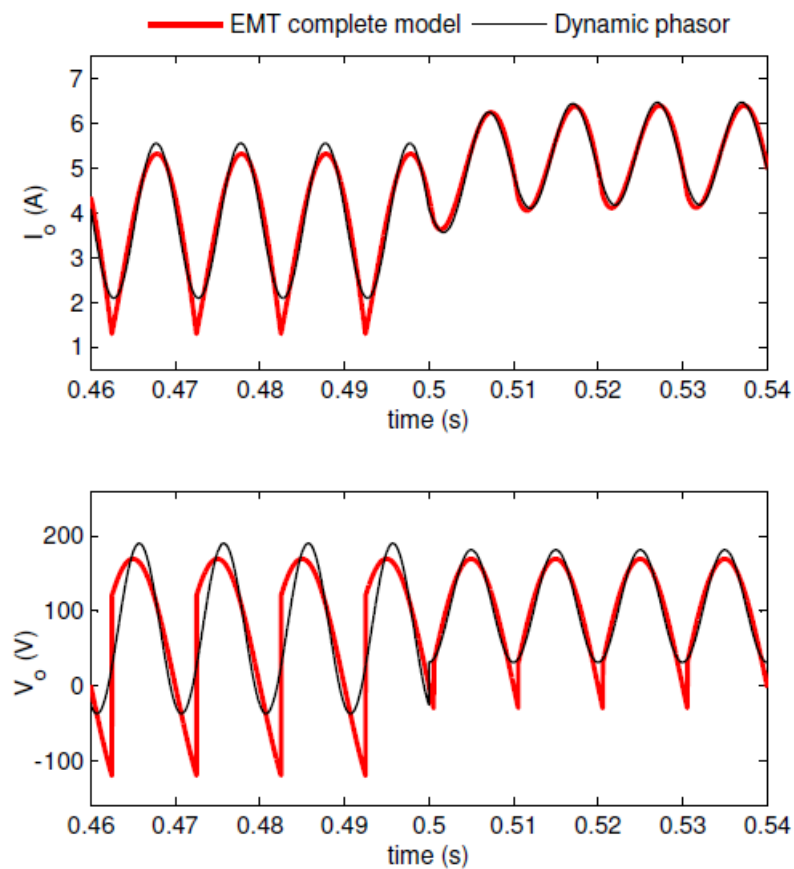


Figure 3.2: Output current (top) and output voltage (bottom).

Figure 3.2 shows a slight difference between the EMT model and dynamic phasor model results. It is because the dynamic phasor model only simulates the lower harmonic spectrum (only the dc and 2nd harmonic components) whereas the EMT program simulates the complete harmonic spectrum; nonetheless the impact of the change in the firing angle from 45° to 10° can be clearly observed in the dynamic phasor model as well as in the EMT results.

Next, the harmonics in the dynamic phasor model are extended up to 20th and the simulation results are compared as in Figure 3.3.

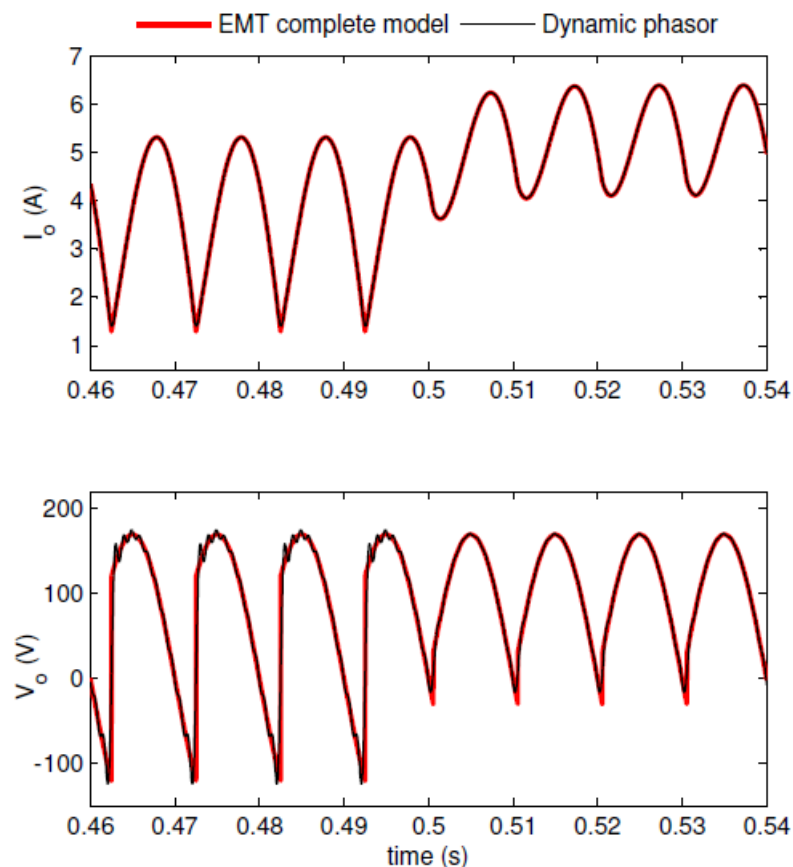


Figure 3.3: Output current (top) and output voltage (bottom) with inclusion of harmonics.

The current waveform of the dynamic phasor model is virtually exactly on top of the results from the PSCAD/EMTDC model. However, in the voltage waveform for a firing angle of 45° , a slight difference is noticed. It is because at a firing angle of 45° , the voltage waveform includes a sharp rise (indicative of a large amount of high frequency components), which requires a larger frequency range than what is considered in the dynamic phasor model.

Figure 3.4 shows the variation of the even harmonics of the output voltage and current obtained through dynamic phasor for firing angle change

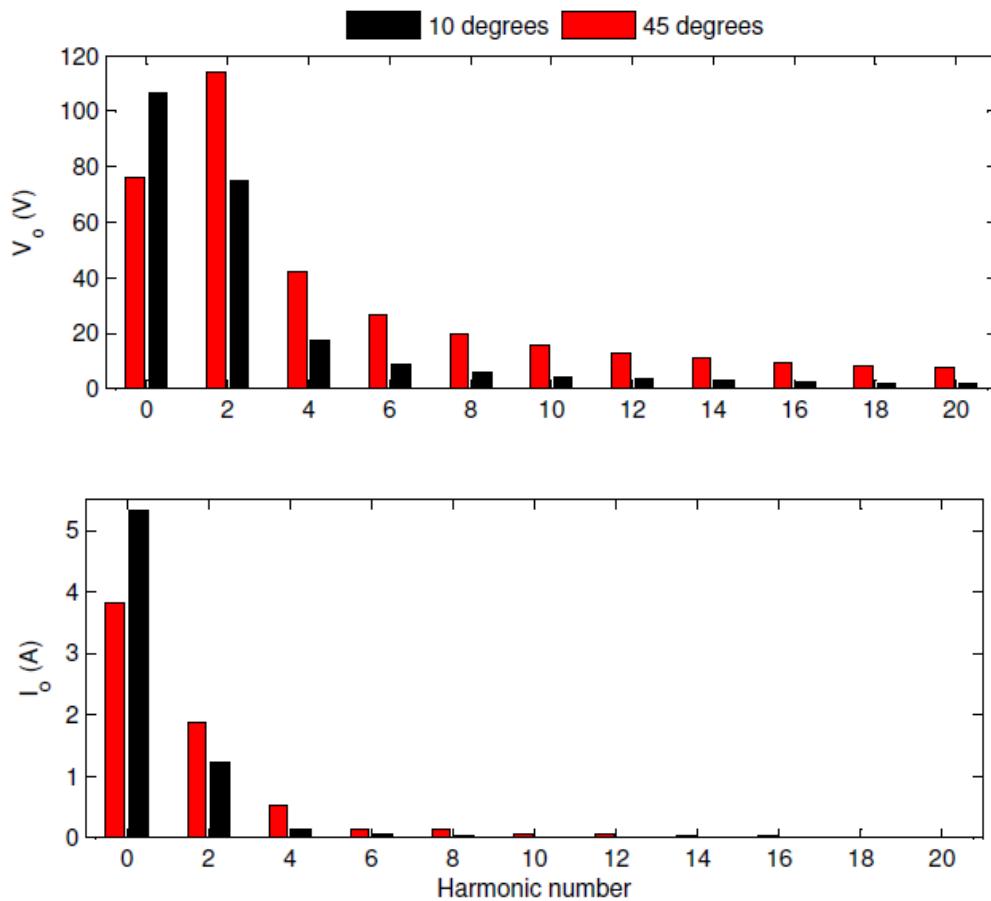


Figure 3.4: Harmonic spectrum of output current (top) and output voltage (bottom) for firing angle change.

Figure 3.4 shows that at 45° , harmonic values of the output voltage are higher than at 10° . In the output current only the dc, 2nd, and 4th harmonics have considerable value.

If more harmonics are added to the dynamic phasor model, voltage and current waveforms with much greater conformity to EMT traces can be obtained. However, compared to the results in Figure 3.2 and Figure 3.3, the accuracy has substantially improved after the addition of harmonics.

3.4 Summary

This chapter presented an introduction to dynamic phasors and the relationship with the harmonics of the system. Dynamic phasor modeling advantages were also mentioned. The basic equations used for dynamic phasor modeling were shown. The dynamic phasor modeling of complex and successfully validated systems available in literature were discussed. Finally, the application of dynamic phasor modeling to a single-phase fully-controlled rectifier was demonstrated; the validated results with EMT by adding some disturbance were also shown.

Chapter 4

Dynamic Phasor Modeling of an MMC

In Chapter 3, dynamic phasor preliminaries were discussed. Additionally a simple converter system was modeled using dynamic phasors to demonstrate how this approach is used in conjunction with switching functions. This chapter mainly focuses on how to develop a dynamic phasor model of an MMC system using dynamic phasors.

An MMC connected to an ac source via a converter transformer is considered in which the MMC acts as an inverter. To develop a dynamic phasor model of this system, mathematical equations of the MMC circuit are necessary. Therefore, firstly the state equations for the MMC are determined using basic circuit laws; then by using dynamic phasor operations, the dynamic phasor equations of MMC are obtained.

4.1 State equations of an MMC

Figure 4.1 shows a schematic diagram of an MMC. By applying KVL to the upper and lower arms as shown in Figure 4.1 with red and green lines, respectively, state equations for the two inductor currents can be found. Then by applying KVL to the

submodule in the upper and lower arms shown in Figure 4.2, two capacitor voltage state equations can be obtained.

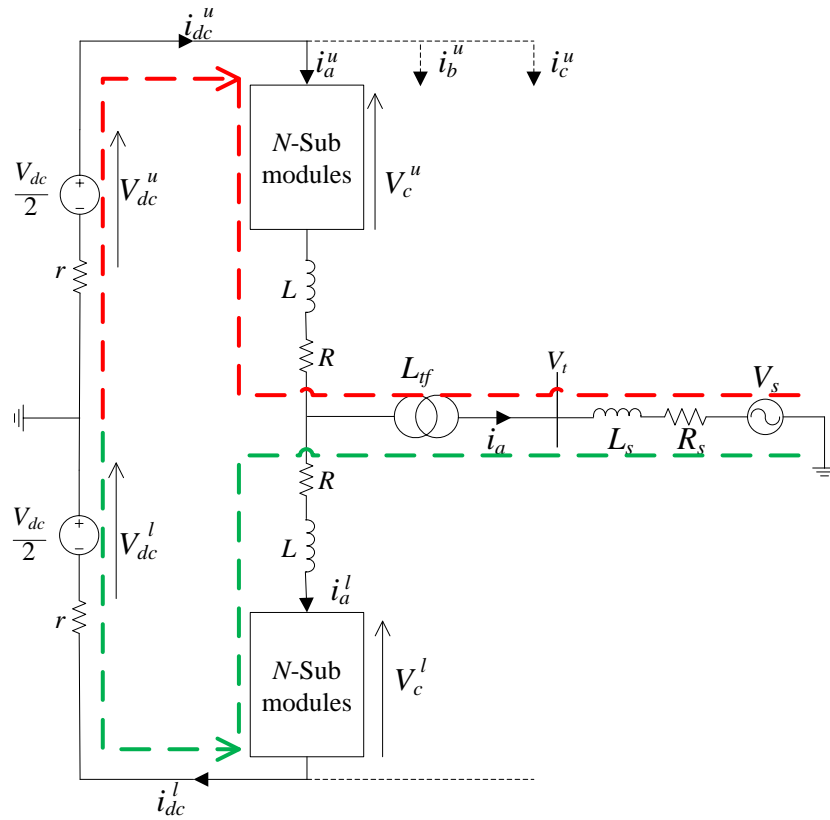


Figure 4.1: Circuit diagram of an MMC.

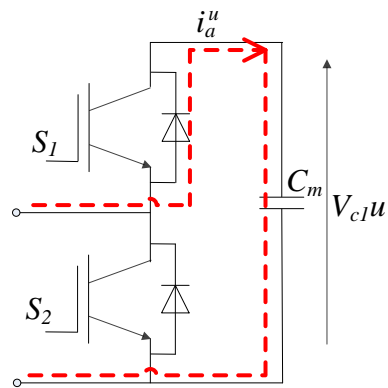


Figure 4.2: Half-bridge submodule circuit.

The equations for the upper and lower arm voltages and currents are shown in (4.1), where $\lambda = a, b, c$ denotes a phase.

$$\begin{aligned}
L \frac{di_{\lambda}^u}{dt} &= V_{dc}^u - ri_{dc}^u - V_{c-\lambda}^u - Ri_{\lambda}^u - (L_s + L_{tf}) \frac{d(i_{\lambda}^u - i_{\lambda}^l)}{dt} - R_s (i_{\lambda}^u - i_{\lambda}^l) - V_{s-\lambda} \\
L \frac{di_{\lambda}^l}{dt} &= V_{dc}^l - ri_{dc}^l - V_{c-\lambda}^l - Ri_{\lambda}^l + (L_s + L_{tf}) \frac{d(i_{\lambda}^u - i_{\lambda}^l)}{dt} + R_s (i_{\lambda}^u - i_{\lambda}^l) + V_{s-\lambda} \\
C_m \frac{dv_{av-\lambda}^u}{dt} &= \frac{n_{\lambda}^u i_{\lambda}^u}{N} \\
C_m \frac{dv_{av-\lambda}^l}{dt} &= \frac{n_{\lambda}^l i_{\lambda}^l}{N} \\
V_{c-\lambda}^u &= n_{\lambda}^u v_{av-\lambda}^u & V_{c-\lambda}^l &= n_{\lambda}^l v_{av-\lambda}^l \\
i_{dc}^u &= i_a^u + i_b^u + i_c^u & i_{dc}^l &= i_a^l + i_b^l + i_c^l
\end{aligned} \tag{4.1}$$

It is seen that the first two state equations in (4.1) include the derivatives of more than one state variable, which does not conform to the conventional form of state space representation. To avoid this, the difference (d) and the sum (s) of the upper-arm (u) and lower-arm (l) currents and voltages are considered. Finally four state equations for the inductor currents and submodule capacitor voltages are found as shown in (4.2).

$$\begin{aligned}
\frac{di_{\lambda}^d}{dt} &= - \left(\frac{R + 2R_s}{L + 2L_{tf} + 2L_s} \right) i_{\lambda}^d + \left(\frac{-ri_{dc}^d - (n_{\lambda}^s v_{av-\lambda}^d + n_{\lambda}^s v_{av-\lambda}^d)/2 - 2V_{s-\lambda}}{L + 2L_{tf} + 2L_s} \right) \\
\frac{di_{\lambda}^s}{dt} &= - \left(\frac{R}{L} \right) i_{\lambda}^s + \left(\frac{V_{dc} - ri_{dc}^s - (n_{\lambda}^s v_{av-\lambda}^s + n_{\lambda}^d v_{av-\lambda}^d)/2}{L} \right)
\end{aligned}$$

$$\frac{dv_{av-\lambda}^d}{dt} = \left(\frac{n_{\lambda}^s i_{\lambda}^d + n_{\lambda}^d i_{\lambda}^s}{2NC_m} \right)$$

$$\frac{dv_{av-\lambda}^s}{dt} = \left(\frac{n_{\lambda}^s i_{\lambda}^s + n_{\lambda}^d i_{\lambda}^d}{2NC_m} \right)$$

$$i_{dc}^d = i_a^d + i_b^d + i_c^d \quad i_{dc}^s = i_a^s + i_b^s + i_c^s \quad (4.2)$$

Here the states are $\langle i_{\lambda}^d \rangle$, $\langle i_{\lambda}^s \rangle$, $\langle v_{av-\lambda}^d \rangle$ and $\langle v_{av-\lambda}^s \rangle$. All other parameters are known; the only unknown functions are the switching functions $\langle n_{\lambda}^d \rangle$, $\langle n_{\lambda}^s \rangle$ which are used to switch the submodules according to the reference waveform. Developing switching functions is discussed in Chapter 5 (Section 5.3).

4.2 Dynamic phasor equations of MMC

The basic dynamic phasor equations shown in (3.2), (3.3), and (3.4) are used to develop the dynamic phasor equations of MMC system given in (4.3).

$$\text{Let, } \beta = \left(\frac{R + 2R_s}{L + 2L_{tf} + 2L_s} \right), \alpha = \left(\frac{1}{L + 2L_{tf} + 2L_s} \right) \text{ and } \gamma = \left(\frac{1}{NC_m} \right), \text{ then}$$

$$\begin{aligned} \frac{d\langle i_{\lambda}^d \rangle_k}{dt} &= -j\omega k \langle i_{\lambda}^d \rangle_k - \beta \langle i_{\lambda}^d \rangle_k \\ &- \alpha \left(r \langle i_{dc}^d \rangle_k + \frac{1}{2} \left(\sum_{l=-\infty}^{+\infty} \langle n_{\lambda}^s \rangle_l \langle v_{av-\lambda}^d \rangle_{k-l} + \sum_{l=-\infty}^{+\infty} \langle n_{\lambda}^d \rangle_l \langle v_{av-\lambda}^s \rangle_{k-l} \right) + 2 \langle V_{s-\lambda} \rangle_k \right) \end{aligned}$$

$$\begin{aligned}
\frac{d\langle i_\lambda^s \rangle_k}{dt} &= -j\omega k \langle i_\lambda^s \rangle_k - \left(\frac{R}{L} \right) \langle i_\lambda^s \rangle_k \\
&+ \frac{1}{L} \left(\langle V_{dc} \rangle_k - r \langle i_{dc}^s \rangle_k - \frac{1}{2} \left(\sum_{l=-\infty}^{+\infty} \langle n_\lambda^s \rangle_l \langle v_{av-\lambda}^s \rangle_{k-l} + \sum_{l=-\infty}^{+\infty} \langle n_\lambda^d \rangle_l \langle v_{av-\lambda}^d \rangle_{k-l} \right) \right) \\
\frac{d\langle v_{av-\lambda}^d \rangle_k}{dt} &= -j\omega k \langle v_{av-\lambda}^d \rangle_k + \frac{\gamma}{2} \left(\sum_{l=-\infty}^{+\infty} \langle n_\lambda^s \rangle_l \langle i_\lambda^d \rangle_{k-l} + \sum_{l=-\infty}^{+\infty} \langle n_\lambda^d \rangle_l \langle i_\lambda^s \rangle_{k-l} \right) \\
\frac{d\langle v_{av-\lambda}^s \rangle_k}{dt} &= -j\omega k \langle v_{av-\lambda}^s \rangle_k + \frac{\gamma}{2} \left(\sum_{l=-\infty}^{+\infty} \langle n_\lambda^s \rangle_l \langle i_\lambda^s \rangle_{k-l} + \sum_{l=-\infty}^{+\infty} \langle n_\lambda^d \rangle_l \langle i_\lambda^d \rangle_{k-l} \right) \quad (4.3)
\end{aligned}$$

For each value of k , the k^{th} harmonics of the currents and voltages are found. One can note that ac side quantities only include odd harmonics and the dc side quantities only include even harmonics. Therefore, for $\langle i_\lambda^d \rangle$ and $\langle v_{av-\lambda}^d \rangle$ states harmonic orders of $k = 1, 3, 5, 7, \dots$ and for $\langle i_\lambda^s \rangle$ and $\langle v_{av-\lambda}^s \rangle$ states harmonic orders of $k = 0, 2, 4, 6, 8, \dots$ are considered. For $k = 0, 1, 2$ the resulting state equations are shown in (4.4).

For $k = 0$,

$$\begin{aligned}
\frac{d\langle i_\lambda^s \rangle_0}{dt} &= -\left(\frac{R}{L} \right) \langle i_\lambda^s \rangle_0 + \frac{1}{L} \left(\langle V_{dc} \rangle_0 - r \langle i_{dc}^s \rangle_0 - \frac{1}{2} \left(\sum_{l=-\infty}^{+\infty} \langle n_\lambda^s \rangle_l \langle v_{av-\lambda}^s \rangle_{-l} + \sum_{l=-\infty}^{+\infty} \langle n_\lambda^d \rangle_l \langle v_{av-\lambda}^d \rangle_{-l} \right) \right) \\
\frac{d\langle v_{av-\lambda}^s \rangle_0}{dt} &= \frac{\gamma}{2} \left(\sum_{l=-\infty}^{+\infty} \langle n_\lambda^s \rangle_l \langle i_\lambda^s \rangle_{-l} + \sum_{l=-\infty}^{+\infty} \langle n_\lambda^d \rangle_l \langle i_\lambda^d \rangle_{-l} \right)
\end{aligned}$$

For $k = 1$,

$$\begin{aligned} \frac{d\langle i_\lambda^d \rangle_1}{dt} &= -j\omega \langle i_\lambda^d \rangle_1 - \beta \langle i_\lambda^d \rangle_1 \\ &- \alpha \left(r \langle i_{dc}^d \rangle_1 + \frac{1}{2} \left(\sum_{l=-\infty}^{+\infty} \langle n_\lambda^s \rangle_l \langle v_{av-\lambda}^d \rangle_{1-l} + \sum_{l=-\infty}^{+\infty} \langle n_\lambda^d \rangle_l \langle v_{av-\lambda}^s \rangle_{1-l} \right) + 2 \langle V_{s-\lambda} \rangle_1 \right) \\ \frac{d\langle v_{av-\lambda}^d \rangle_1}{dt} &= -j\omega \langle v_{av-\lambda}^d \rangle_1 + \frac{\gamma}{2} \left(\sum_{l=-\infty}^{+\infty} \langle n_\lambda^s \rangle_l \langle i_\lambda^d \rangle_{1-l} + \sum_{l=-\infty}^{+\infty} \langle n_\lambda^d \rangle_l \langle i_\lambda^s \rangle_{1-l} \right) \end{aligned}$$

For $k = 2$,

$$\begin{aligned} \frac{d\langle i_\lambda^s \rangle_2}{dt} &= -2j\omega \langle i_\lambda^s \rangle_2 - \left(\frac{R}{L} \right) \langle i_\lambda^s \rangle_2 \\ &- \frac{1}{L} \left(r \langle i_{dc}^s \rangle_2 + \frac{1}{2} \left(\sum_{l=-\infty}^{+\infty} \langle n_\lambda^s \rangle_l \langle v_{av-\lambda}^s \rangle_{2-l} + \sum_{l=-\infty}^{+\infty} \langle n_\lambda^d \rangle_l \langle v_{av-\lambda}^d \rangle_{2-l} \right) \right) \\ \frac{d\langle v_{av-\lambda}^s \rangle_2}{dt} &= -2j\omega \langle v_{av-\lambda}^s \rangle_2 + \frac{\gamma}{2} \left(\sum_{l=-\infty}^{+\infty} \langle n_\lambda^s \rangle_l \langle i_\lambda^s \rangle_{2-l} + \sum_{l=-\infty}^{+\infty} \langle n_\lambda^d \rangle_l \langle i_\lambda^d \rangle_{2-l} \right) \end{aligned} \quad (4.4)$$

All non-zero harmonic orders have real and imaginary components; also each harmonic is present in all three phases. Therefore, the equations shown in (4.4) need to be separated into real and imaginary parts for phases a, b, and c as shown below.

Let,

$$x_{1\lambda} = \langle i_\lambda^s \rangle_0$$

$$x_{2\lambda} = \langle V_{av-\lambda}^s \rangle_0$$

$$x_{3\lambda} + jx_{4\lambda} = \text{Re} \langle i_\lambda^d \rangle_1 + j \text{Im} \langle i_\lambda^d \rangle_1$$

$$x_{5\lambda} + jx_{6\lambda} = \text{Re} \langle V_{av-\lambda}^d \rangle_1 + j \text{Im} \langle V_{av-\lambda}^d \rangle_1$$

$$\begin{aligned}
x_{7\lambda} + jx_{8\lambda} &= \text{Re}\langle i_{\lambda}^s \rangle_2 + j \text{Im}\langle i_{\lambda}^s \rangle_2 \\
x_{9\lambda} + jx_{10\lambda} &= \text{Re}\langle V_{av-\lambda}^s \rangle_2 + j \text{Im}\langle V_{av-\lambda}^s \rangle_2
\end{aligned} \tag{4.5}$$

This shows that to develop a model for the MMC including up to the 2nd harmonic as shown in (4.4), 30 state variables (and hence 30 state equations) are needed. From the state equations, a matrix can be constructed in the following form.

$$\dot{X} = AX + BU \tag{4.6}$$

where A and B are constant matrices, U is the input, and X is the state vector. A numerical integration method is needed to solve (4.6). If more harmonics are added to the dynamic phasor model, the number of state equations will increase accordingly.

4.3 Solving dynamic phasor equations

4.3.1 Selection of a numerical integration method

There are several integration methods available to solve state equations. Two of these are the rectangular integration and the trapezoidal integration methods. The trapezoidal method preserves stability for linear systems and features better accuracy than the rectangular method [40]. Therefore, the trapezoidal method is chosen for this research. A brief description of this integration method is given next.

4.3.2 Trapezoidal method of integration

Consider a state equation as shown in (4.7).

$$\frac{dx(t)}{dt} = Ax(t) + Bu(t)$$

$$x(t) = x(t - \Delta t) + \int_{t-\Delta t}^t (Ax(t) + Bu(t)) dt \quad (4.7)$$

It is desired to numerically solve this equation using a small time-step of Δt . The trapezoidal rule can be applied as shown in (4.8).

$$x(t) = x(t - \Delta t) + A \left(\frac{x(t) + x(t - \Delta t)}{2} \right) \Delta t + B \left(\frac{u(t) + u(t - \Delta t)}{2} \right) \Delta t$$

$$x(t) \left(I - \frac{A\Delta t}{2} \right) = x(t - \Delta t) \left(I + \frac{A\Delta t}{2} \right) + B\Delta t \left(\frac{u(t) + u(t - \Delta t)}{2} \right)$$

$$x(t) = \left(I - \frac{A\Delta t}{2} \right)^{-1} \left(I + \frac{A\Delta t}{2} \right) x(t - \Delta t) + B\Delta t \left(I - \frac{A\Delta t}{2} \right)^{-1} u(t)$$

$$x(t) = Gx(t - \Delta t) + Hu(t)$$

$$\text{where } G = \left(I - \frac{A\Delta t}{2} \right)^{-1} \left(I + \frac{A\Delta t}{2} \right) \text{ and } H = B\Delta t \left(I - \frac{A\Delta t}{2} \right)^{-1} \quad (4.8)$$

The formulation shown in (4.8) is used to solve the state equations of the MMC. If the number of harmonics included is large, then the number of dynamic phasor equations will be accordingly large; therefore, the size of the system matrix will be large. By choosing a suitable time-step the matrix can be solved.

Typically the time-step should be less than the 1/10 of the period of the highest frequency in the system response or the smallest time constant in the circuit as a rule of thumb. However, this is not always known beforehand; therefore, selection of a simulation time-step is often a matter of trial and error, wherein several values are tried before a suitable value is obtained [40].

4.4 Summary

In this chapter, obtaining state equations for a MMC circuit by using state space equations was discussed. Then dynamic phasor equations of MMC using dynamic phasor preliminaries, for extended harmonics, were derived. As an example for harmonic number $k = 0, 1, 2$ DP equations of the MMC were shown. Next constructing the equations into a matrix was shown. Finally by selecting a suitable numerical integration method and a time-step, solving the matrix was explained. Dynamic phasor models of direct controller and PLL are explained in the next chapter.

Chapter 5

Dynamic Phasor Modeling of the Converter Control System

Generally, the converters in an HVDC network maintain such variables as the ac voltage, reactive power, dc voltage, or real power. In this research the terminal real power and terminal RMS voltage are the two parameters regulated by the MMC control system. The direct control method is selected to control the MMC due to simplicity and effectiveness. To control the system, a PLL is used to track the ac voltage at the point of common coupling. Therefore, a dynamic phasor model of the direct control system and the PLL are needed to be developed and interfaced with the MMC model.

5.1 Modeling of power and voltage controllers

To control the real power flow and the terminal RMS voltage in the dynamic phasor model of MMC, the direct control technique is selected and implemented using extended-frequency dynamic phasors. In this control method, there are only two controllers

(proportional-integral (PI) controllers are adopted here): one to control the real power by changing the phase angle (δ), and the other to regulate the terminal voltage by adjusting the modulation index (m) as shown in Figure 5.1. Therefore, the number of state equations will be fewer than a decoupled controller and as such the tuning of the controller is also easy.

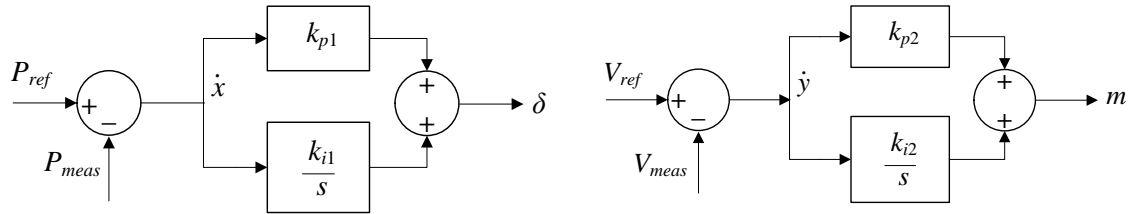


Figure 5.1: Block diagram of the direct controller: (a) real power controller, (b) terminal voltage controller.

As shown in Figure 5.1, the errors between the references and the actual variables of interest are fed through PI controllers that eventually generate commands for the converter's modulation index and phase shift in order to make their errors to approach zero. The converter's output voltage phase-shift is relative to a reference sinewave that is achieved using a phase-locked loop (PLL) unit connected to the point of common coupling (PCC). The controller inputs are the reference values of the real power and the RMS terminal voltage; the controller outputs are also (quasi-)dc quantities. As such in their dynamic phasor model, inclusion of harmonics is not necessary.

5.1.1 Real power controller

From Figure 5.1(a), the state equation for the real power controller can be obtained as given in (5.1).

$$\frac{dx}{dt} = P_{ref} - P_{meas}$$

$$\delta = k_{p2} \frac{dx}{dt} + k_{i2} x \quad (5.1)$$

Real power flow comprises of a primarily dc component. Therefore, only one δ value is needed (i.e., no harmonic order model for the PI controller is developed); P_{ref} is the ordered power, and the actual power is determined as follows.

$$P_{meas} = V_{ta}.i_a + V_{tb}.i_b + V_{tc}.i_c \quad (5.2)$$

The dynamic phasor equation of the actual power is given in (5.3).

$$\langle P_{meas} \rangle_k = \sum_{l=-\infty}^{\infty} \langle V_{ta} \rangle_l \langle i_a \rangle_{k-l} + \sum_{l=0}^{\infty} \langle V_{tb} \rangle_l \langle i_b \rangle_{k-l} + \sum_{l=0}^{\infty} \langle V_{tc} \rangle_l \langle i_c \rangle_{k-l}$$

$$\langle P_{meas} \rangle_0 = \sum_{l=-\infty}^{\infty} \langle V_{ta} \rangle_l \langle i_a \rangle_{-l} + \langle V_{tb} \rangle_l \langle i_b \rangle_{-l} + \langle V_{tc} \rangle_l \langle i_c \rangle_{-l} \quad (5.3)$$

Using the terminal voltage and current, the actual power can be found from equation (5.3). It is assumed that the fundamental terminal voltages and currents are adequate to find δ , as products of the other odd harmonics are considerably smaller.

$$\langle P_{meas} \rangle_0 = \langle V_{ta} \rangle_1 \langle i_a \rangle_{-1} + \langle V_{ta} \rangle_{-1} \langle i_a \rangle_1 + \langle V_{tb} \rangle_1 \langle i_b \rangle_{-1} + \langle V_{tb} \rangle_{-1} \langle i_b \rangle_1 + \langle V_{tc} \rangle_1 \langle i_c \rangle_{-1} + \langle V_{tc} \rangle_{-1} \langle i_c \rangle_1$$

$$\langle P_{meas} \rangle_0 = 2 \begin{pmatrix} \text{Re} \langle V_{ta} \rangle_1 \text{Re} \langle i_a \rangle_1 + \text{Im} \langle V_{ta} \rangle_1 \text{Im} \langle i_a \rangle_1 \\ + \text{Re} \langle V_{tb} \rangle_1 \text{Re} \langle i_b \rangle_1 + \text{Im} \langle V_{tb} \rangle_1 \text{Im} \langle i_b \rangle_1 \\ + \text{Re} \langle V_{tc} \rangle_1 \text{Re} \langle i_c \rangle_1 + \text{Im} \langle V_{tc} \rangle_1 \text{Im} \langle i_c \rangle_1 \end{pmatrix} \quad (5.4)$$

The reference power is defined by the user (or an upstream control system), and the output δ can be found using (5.1). The angle δ is then used in the fundamental component of the switching signal to regulate the real power to the ordered value.

5.1.2 Terminal RMS voltage controller model

The state equation of the voltage controller is obtained from the control block diagram shown in Figure 5.1(b) as follows.

$$\frac{dy}{dt} = V_{ref} - V_{meas}$$

$$m = k_{p2} \frac{dy}{dt} + k_{i2} y \quad (5.5)$$

The terminal voltage is a staircase waveform obtained by stacking the voltages of an appropriate number of submodules; due to its quarter-cycle symmetry, it only contains odd harmonics. The controller input V_{meas} is the line to line RMS value. General line to line RMS voltage calculation method for a 3-phase system in time domain is shown in (5.6).

$$V_{rms} = \sqrt{\frac{(V_{ta} - V_{tb})^2 + (V_{tb} - V_{tc})^2 + (V_{tc} - V_{ta})^2}{3}}$$

$$V_{rms} = \sqrt{\frac{V_{tab}^2 + V_{tbc}^2 + V_{tca}^2}{3}} \quad (5.6)$$

The real and imaginary values of the terminal voltage for each harmonic are known, and the basic RMS equation and the corresponding dynamic phasor equation are given in (5.6). Note that V_{rms} represents a dc value (magnitude) for each harmonic order k .

$$\begin{aligned}\langle V_{rms} \rangle_k &= \sqrt{\frac{\sum_{l=-\infty}^{\infty} (\langle V_{tab} \rangle_l \langle V_{tab} \rangle_{k-l} + \langle V_{tbc} \rangle_l \langle V_{tbc} \rangle_{k-l} + \langle V_{tca} \rangle_l \langle V_{tca} \rangle_{k-l})}{3}} \\ \langle V_{rms} \rangle_0 &= \sqrt{\frac{\sum_{l=-\infty}^{\infty} (\langle V_{tab} \rangle_l \langle V_{tab} \rangle_{-l} + \langle V_{tbc} \rangle_l \langle V_{tbc} \rangle_{-l} + \langle V_{tca} \rangle_l \langle V_{tca} \rangle_{-l})}{3}}\end{aligned}\quad (5.7)$$

For each odd value of l , the magnitude of the l -th harmonic RMS voltage can be found. Generally, resultant RMS value obtained through the sum of RMS values of the each harmonics; as shown in (5.7).

The RMS value of V_{meas} for odd harmonics can be found as follows. Here the conjugate of the l -th harmonic also needs to be considered.

$$\langle V_{meas} \rangle_l = \sqrt{\frac{\langle V_{tab} \rangle_l \langle V_{tab} \rangle_{-l} + \langle V_{tbc} \rangle_l \langle V_{tbc} \rangle_{-l} + \langle V_{tca} \rangle_l \langle V_{tca} \rangle_{-l}}{3}}\quad (5.8)$$

As an example V_{meas} for the fundamental component can be found as follows.

$$\begin{aligned}\langle V_{meas} \rangle_1 &= \sqrt{\frac{\langle V_{tab} \rangle_1 \langle V_{tab} \rangle_{-1} + \langle V_{tbc} \rangle_1 \langle V_{tbc} \rangle_{-1} + \langle V_{tca} \rangle_1 \langle V_{tca} \rangle_{-1} + \langle V_{tab} \rangle_{-1} \langle V_{tab} \rangle_1 + \langle V_{tbc} \rangle_{-1} \langle V_{tbc} \rangle_1 + \langle V_{tca} \rangle_{-1} \langle V_{tca} \rangle_1}{3}} \\ \langle V_{meas} \rangle_1 &= \sqrt{\frac{2(\operatorname{Re}\langle V_{tab} \rangle_1^2 + \operatorname{Im}\langle V_{tab} \rangle_1^2 + \operatorname{Re}\langle V_{tbc} \rangle_1^2 + \operatorname{Im}\langle V_{tbc} \rangle_1^2 + \operatorname{Re}\langle V_{tca} \rangle_1^2 + \operatorname{Im}\langle V_{tca} \rangle_1^2)}{3}}\end{aligned}$$

If the equation is further simplified by considering the a-phase voltage, then

$$\langle V_{meas} \rangle_1 = \sqrt{2 \times 3 (\operatorname{Re} \langle V_{ta} \rangle_1^2 + \operatorname{Im} \langle V_{ta} \rangle_1^2)} \quad (5.9)$$

If it is written in a general form for the k^{th} harmonic magnitude,

$$\langle V_{meas} \rangle_k = \sqrt{\frac{3}{2}} \cdot 2 \sqrt{(\operatorname{Re} \langle V_{ta} \rangle_k)^2 + (\operatorname{Im} \langle V_{ta} \rangle_k)^2} \quad (5.10)$$

It can be simply modified as follows, which is the basic form normally used to find the RMS voltage.

$$\langle \langle V_{meas} \rangle_k \rangle_{rms} = \sqrt{\frac{3}{2}} \cdot \langle \langle V_{ta} \rangle_k \rangle_{peak} \quad (5.11)$$

The dynamic phasor form of (5.5) is shown in (5.12). Note that the output modulation indices for each harmonic are also dc values.

$$\begin{aligned} \left\langle \frac{dy}{dt} \right\rangle_k &= \langle V_{ref} \rangle_k - \langle V_{meas} \rangle_k \\ \langle m \rangle_k &= k_{p2} \left\langle \frac{dy}{dt} \right\rangle_k + k_{i2} \langle y \rangle_k \end{aligned} \quad (5.12)$$

In (5.12) the only unknown parameter is V_{ref} to find the modulation indices. To find the reference values for each harmonic, the nearest level control is used, which is discussed in the next section.

5.1.3 Nearest level control and voltage reference

The MMC control system determines the fundamental value of V_{ref} and from that a staircase voltage waveform closely resembling a sinewave with such magnitude must be generated. Nearest level control technique is used to generate the staircase waveform for the corresponding sine waveform (as explained in section 2.2.2).

The switching instants between levels are called as the nearest level angles. By using Fourier expansion (see (3.2)) for each value of k , the k^{th} Fourier coefficient can be calculated as follows.

$$C_k = \frac{1}{2\pi} \int_0^{2\pi} V_{out} e^{-jk\theta} d\theta$$

where V_{out} is the staircase waveform obtained through NLC. Then,

$$\langle V_{ref} \rangle_k = 2|C_k| \quad (5.13)$$

V_{ref} can be converted to line-to-line RMS and given as the reference voltage for each harmonic in the voltage controller. Using (5.12) for each odd harmonic, the modulation index value (m) corresponding to each harmonic can be obtained. By using the modulation index values in the switching signal, the terminal voltage can be regulated.

5.2 Dynamic phasor modeling of PLL

A PLL is a feedback control system that is used to track the phase angle of a given sinusoidal voltage. A dynamic phasor model of the PLL is developed in [11], [41] and

has been used for this research. Figure 5.2, shows the block diagram of the phasor model of a PLL.

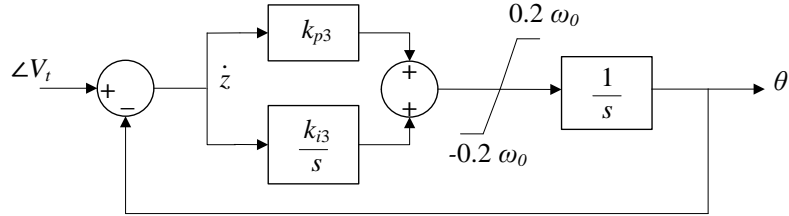


Figure 5.2: Block diagram of phasor model of PLL.

The state equations for a PLL can be obtained from Figure 5.2, as given in (5.14).

$$\frac{dz}{dt} = \angle V_t - \theta$$

$$\frac{d\theta}{dt} = k_{p3}(\angle V_t - \theta) + k_{i3}z \quad (5.14)$$

Phase angle of V_t is found using the real and imaginary components of terminal voltage. The output angle θ is a dc value; therefore, to obtain the dynamic phasor equations, $k=0$ is only considered. Note that the phase angle θ is the voltage angle related to global reference, which is connected to the terminal point of the converter.

5.3 Switching signal generation

To generate the switching signals for the upper and lower arms, the modulation index and the phase angle from the direct controller and the PLL angle are required. The upper-arm and lower-arm switching signals for phase ‘a’ (in time domain) are given in (5.15).

$$\begin{aligned}
n_a^u &= \frac{N}{2} - \frac{N}{2} \sum_{k=1}^{\infty} \langle m \rangle_k \sin(k\omega t + k\theta + \delta_k) \\
n_a^l &= \frac{N}{2} + \frac{N}{2} \sum_{k=1}^{\infty} \langle m \rangle_k \sin(k\omega t + k\theta + \delta_k)
\end{aligned} \tag{5.15}$$

where k is an odd number. For phases ‘b’ and ‘c’, phase shifts of 120° and 240° need to be added, respectively. Since the difference and sum of the switching signals are used in equations (4.2) and (4.3), the sum and difference of the switching signals in equation (5.15) need to be obtained as follows.

$$\begin{aligned}
n_a^d &= -N \sum_{k=1}^{\infty} \langle m \rangle_k \sin(k\omega t + k\theta + \delta_k) \\
n_a^s &= N
\end{aligned} \tag{5.16}$$

As it can be seen from (5.16), the sum of the switching signals is a constant and is equal to the number of submodules per arm of the MMC. The only time variant part is the difference of the switching signals. Firstly, the equation shown in (5.16) can be expanded as follows.

$$n_a^d = -N \left\{ \langle m \rangle_1 \sin(\omega t + \theta + \delta_1) + \langle m \rangle_3 \sin(3\omega t + 3\theta + \delta_3) + \langle m \rangle_5 \sin(5\omega t + 5\theta + \delta_5) + \dots \right\} \tag{5.17}$$

Using dynamic phasor’s basic equations, the dynamic phasor representation of (5.17) can be found as given in (5.18).

$$\langle n_a^d \rangle_k = -\frac{N\langle m \rangle_k}{2j} e^{j(k\theta + \delta_k)} = \frac{jN\langle m \rangle_k}{2} e^{j(k\theta + \delta_k)} \quad (5.18)$$

Similarly, the switching signals corresponding to other two phases can be obtained. For odd values of k , the k^{th} harmonic of the switching signal can be obtained. As mention in section 5.1.1 real power is a dc value therefore only one δ for the fundamental was found.

5.4 Summary

In this chapter, developing a dynamic phasor model of the real-power and voltage controllers in the direct controller method to regulate terminal real power and terminal RMS voltage was discussed. Then the use of the nearest level control method for finding voltage references for each harmonics was explained. The application of the dynamic phasor model of PLL in MMC was mentioned. Finally, it was shown how to find the k^{th} switching signal from the PLL angle θ and direct control outputs δ and m .

Chapter 6

Validation of the Dynamic Phasor

Model of the MMC

Electromagnetic transient (EMT) simulation programs such as PSCAD/EMTDC are widely used to study fast transients that occur in power systems with embedded power electronics. Due to their detailed models and accurate solution methods, EMT simulation results are generally taken to be close representations of the real phenomena, and as such it is common to use them as benchmarks for validation of other types of models. This thesis develops a detailed switching model of MMC test system in EMTDC/PSCAD for use as a benchmark to assess and validate the dynamic phasor models developed in the previous chapters.

6.1 MMC test system specifications

The simulated circuit's parameters are given in Table 6.1. The number of levels in the MMC is intentionally selected to be small ($N=5$) so that the staircase nature of the output

voltage is evident in the EMT results for better comparability. The number of submodules is limited in EMT design of MMC because; the complexity of MMC circuitry and the presence of a large number of switches pose major computational difficulties for their EMT simulation. It is often observed that simplifications need to be made in order to enable EMT simulation of MMC systems within reasonable computing time. As such average-value modeling has been a practice of choice [42]-[43].

In addition, to minimize the burden on modeling, large submodule capacitors (5000 μF) are selected so that the effect of circulating currents becomes minimal.

Table 6.1: MMC system parameters

Parameter	Value
AC system's rated voltage	290 kV
Short circuit ratio	4.0 $\angle 80^\circ$
Converter transformer turns ratio	290:290
Converter transformer impedance	0.05 pu on 700 MVA
Power rating	500 MW
Rated dc voltage, internal resistance	500 kV, 0.001 Ω
Arm inductor	0.001 H
Submodule capacitor	5000 μF
Nominal Voltage of Submodule capacitor	100 kV

As mentioned in Chapter 5, the direct controller is developed to control the terminal real power (P) and RMS voltage (V). The parameters of the PI controllers used in PV control and PLL parameters are given in Table 6.2. The values of proportional (k_p) and integral gain (k_i) are selected based on trial and error.

Table 6.2: Controller parameters

Controllers	Gain	
	k_p	k_i
PLL	50	900
Real power controller	0.04	0.25
Terminal voltage controller	0.005	50

6.2 Electromagnetic transient simulation model

The simulated MMC converter consists of three phases and each phase consists of two arms. Each arm is constructed by cascading 5 half-bridge submodules. The AC side of the converter is connected to an AC power system through a three-phase converter transformer. The AC power system is modeled using a voltage source behind a Thevenin impedance. To control the ac voltage and real power at the point of common coupling (PCC), the direct control method is utilized. Output signals from the direct controller and the PLL are combined to produce reference signals for the MMC. Then, the nearest level control is used to generate the upper and lower arm switching signals from the reference signals; capacitor voltage balancing is used to switch the submodules in a proper way according to the direction of corresponding arm currents. The operation of the MMC circuit used here is explained in the complete block diagram shown in Figure 6.1.

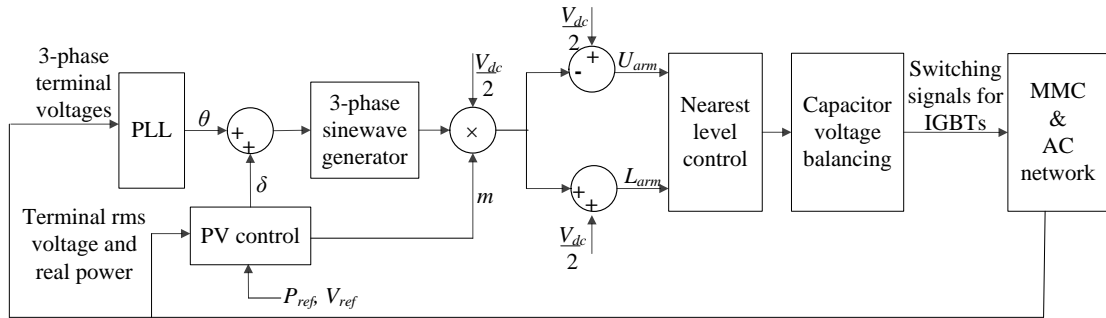


Figure 6.1: Block diagram of the MMC system.

EMT modeling is done using PSCAD/EMTDC's master library components and user-defined components. The user-defined components are written using the FORTRAN programming language to perform the nearest level control and the capacitor voltage balancing operations.

In EMT simulation technique, circuits are solved using nodal analysis technique that converts the circuit into current sources and conductance. Then, by applying Kirchhoff's current law (KCL) to each node, the nodal equations are written and solved using a proper numerical integration technique. Typically, the trapezoidal integration method is used in EMT simulation as it preserves numerical stability for linear systems and allows use of larger time-steps than Euler's method [44].

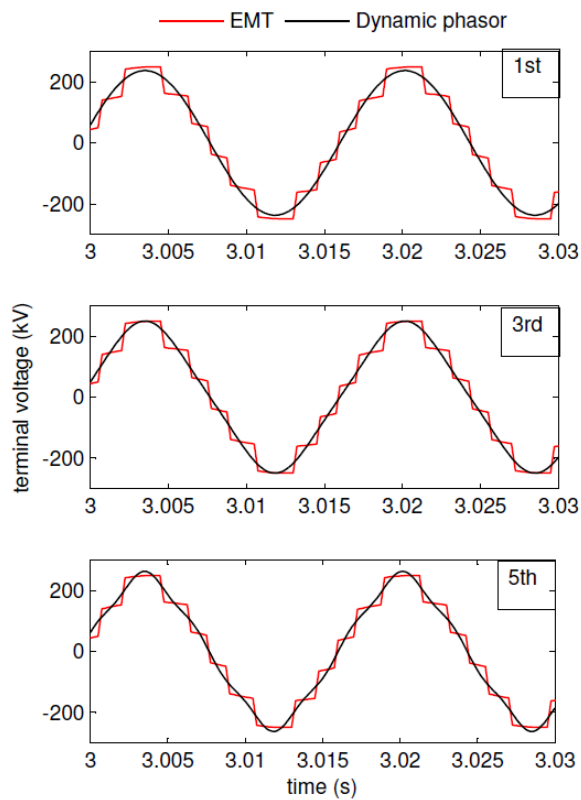
6.3 Comparison of simulation results

The parameters of the extended-frequency dynamic phasor model developed in MATLAB are selected identical to that of the EMT simulation model. The results from dynamic phasor model and EMT model are compared at steady state and during transients by applying identical disturbances to both models. The time-domain simulation

results provided in the following sections consist of EMT simulation results that are obtained with a 50- μ s time-step and dynamic phasor simulation results that are with a 100- μ s time-step.

6.3.1 Simulation results at steady state

In Figure 6.2, the dynamic phasor model results and complete EMT model results are compared. Figures show a progressive addition of odd harmonics to the dynamic phasor model and how doing so contributes to the improved accuracy of the model.



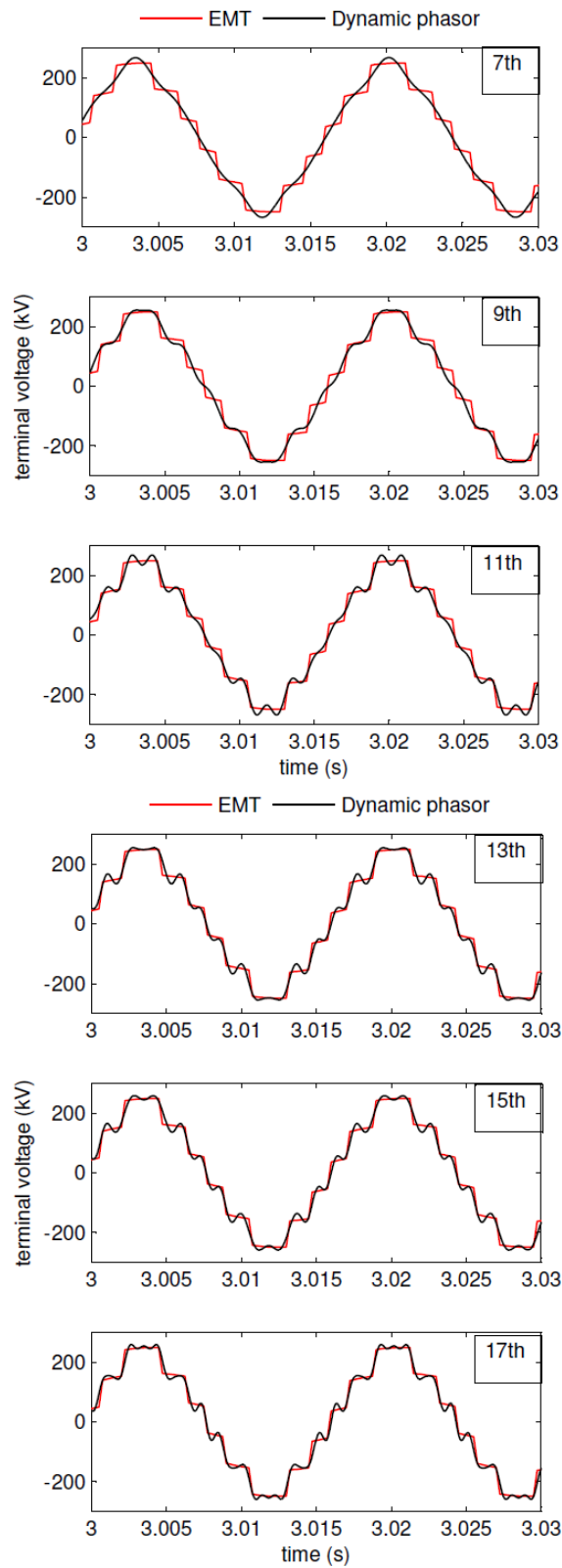


Figure 6.2: Progressive harmonic addition to the dynamic phasor model and comparison with the EMT.

From Figure 6.2, the influence of odd harmonics on the reconstructed staircase voltage waveform can be observed. Further, it can be noticed that the addition of each odd harmonic improves the voltage waveform as it becomes closer to the EMT result, which includes all the harmonics. The first few harmonics do not seem to add much to the accuracy of the results, because the original staircase waveform with the chosen number of levels does not have much low-frequency contents.

Figure 6.3 shows the harmonic values in a 5-level stair case waveform.

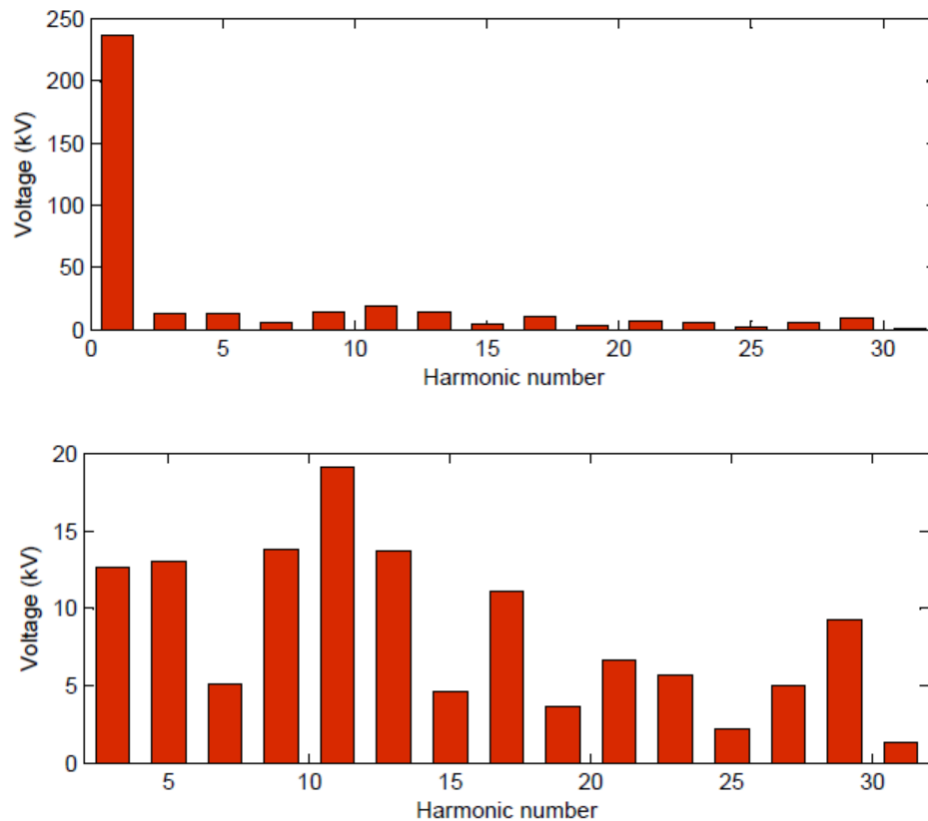


Figure 6.3: (Top) Harmonic spectrum of the terminal voltage of 5-level converter (bottom) Zoomed version of the spectrum excluding the fundamental.

From Figure 6.3, it can be noticed that the dominant harmonic after the fundamental, is the 11th harmonic. In addition 3rd, 5th, 9th, 13th and 17th harmonics cannot be completely

neglected. The presence of the above harmonics is the cause for the staircase shape of the voltage waveform as shown in Figure 6.2. The dominant harmonic may vary with the use of different number of submodules.

Figure 6.4 compares the simulated results of phase-a voltage and current from both models at steady state.

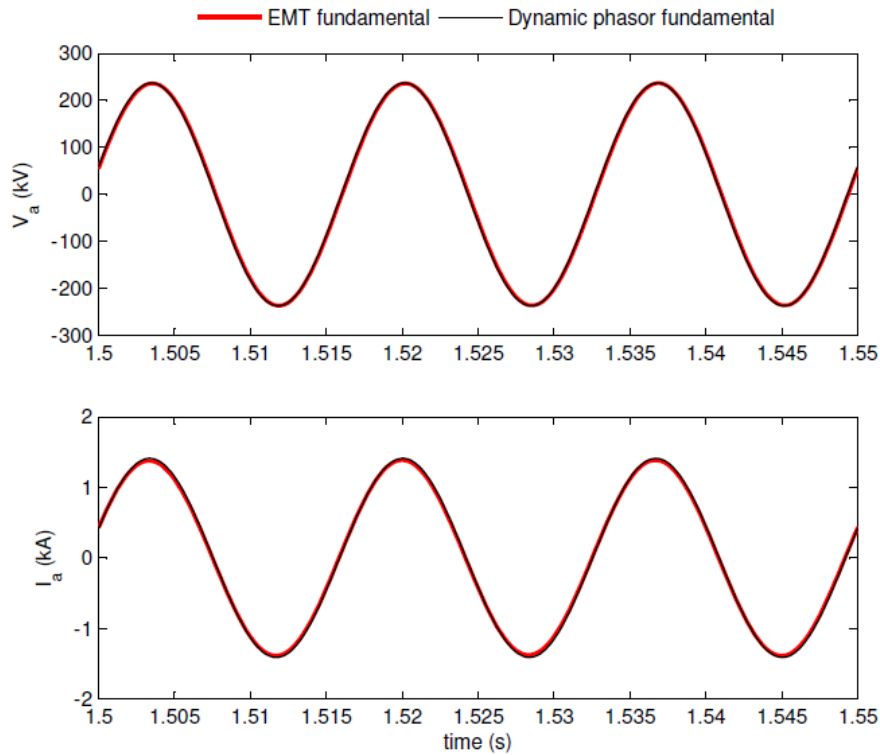


Figure 6.4: Comparison of voltage (top) and current (bottom) at steady state fundamental only.

Although the EMT simulation results include all harmonics, the fundamental components of the waveforms can be extracted using a standard fast Fourier transform (FFT) block available in PSCAD/EMTDC. The dynamic phasor simulation results in Figure 6.4 only include the fundamental. It can be observed that results from both models are well matched.

To investigate the improvement in model accuracy with the addition of harmonics, the dynamic phasor model is developed including all odd harmonics up to 17th. The results from dynamic phasor model are compared with the results from the complete EMT model in Figure 6.5.

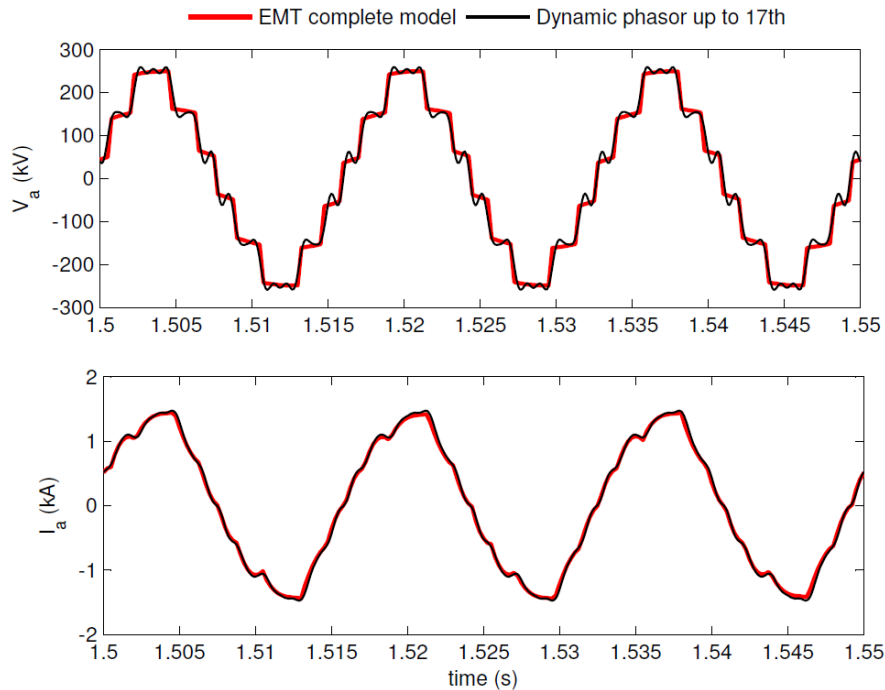


Figure 6.5: Comparison of voltage (top) and current (bottom) at steady state with harmonics.

From above simulation results, one can notice that when a larger number of harmonics are added to the dynamic phasor model, a closer match with the EMT simulation results can be obtained. However, even with the inclusion of harmonics up to 17th, the dynamic phasor results show a close match with the EMT simulation results.

To further analyze the accuracy of the dynamic phasor model, in the EMT model, using the FFT block and the addition block, a waveform is constructed by adding odd

harmonics up to 17th in PSCAD/EMTDC. The simulation results are compared in Figure 6.6.

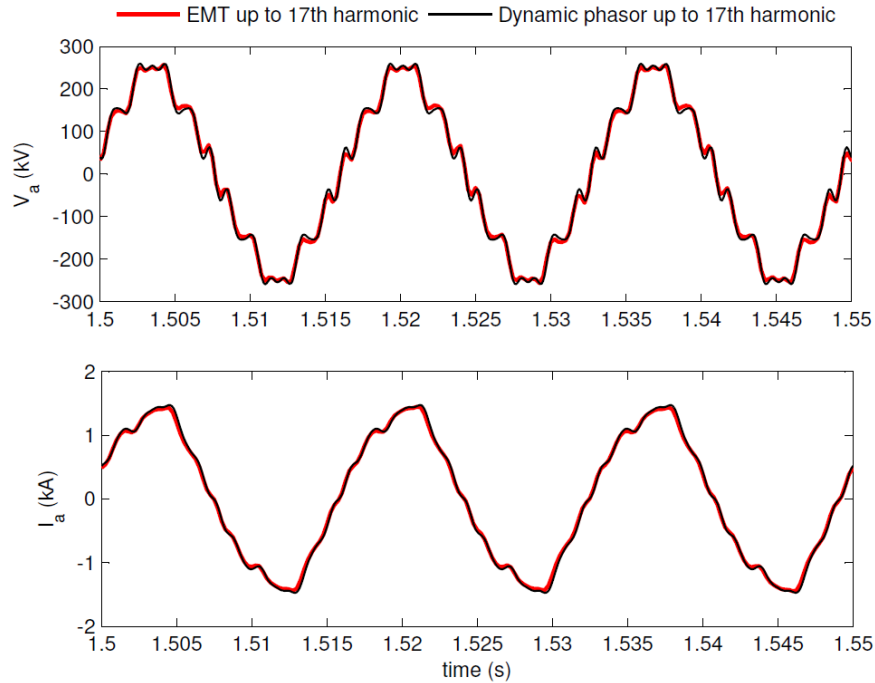


Figure 6.6: Comparison of voltage (top) and current (bottom) at the steady state with inclusion of harmonics up to 17th in both models.

From Figure 6.6, it is clear that results from both models match well.

6.3.2 Simulation results for a step change in voltage reference

A step decrease from 1 p.u. to 0.75 p.u. is applied to the terminal ac voltage reference at 2.0 s. The smooth RMS voltage transition obtained through the voltage controller in dynamic phasor model is shown in Figure 6.7.

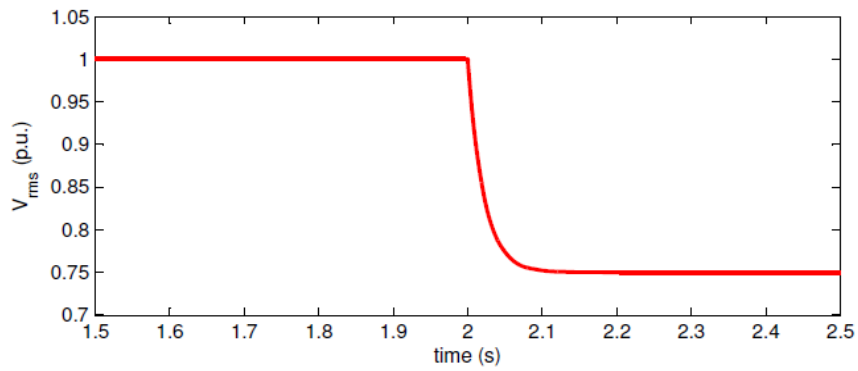


Figure 6.7: Response to a step change in terminal voltage.

Figure 6.8 shows the comparison of fundamental results from the EMT model and the dynamic phasor model for the step change in voltage.

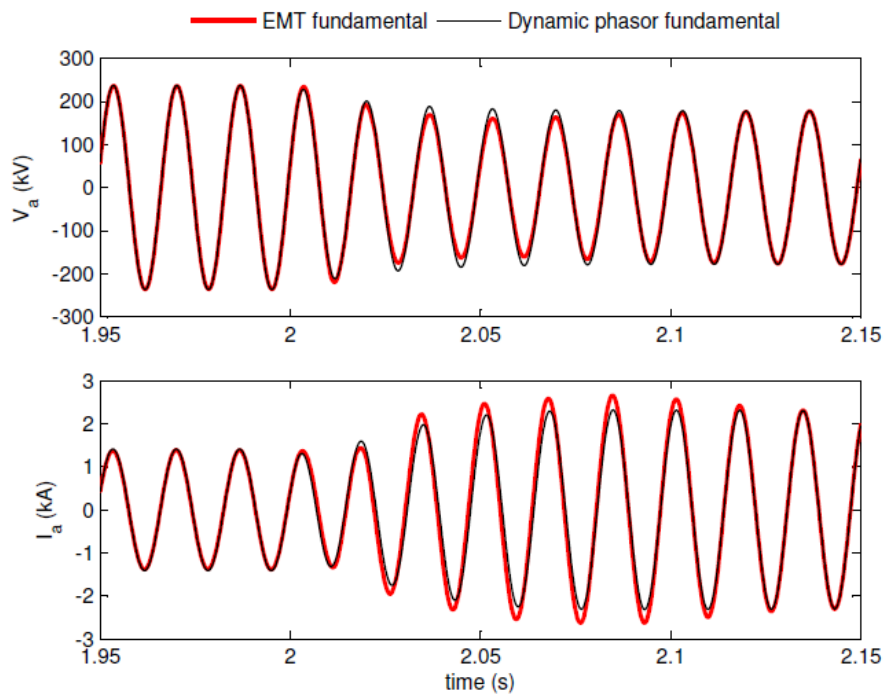


Figure 6.8: Comparison of voltage (top) and current (bottom) fundamental only to a step change in the voltage reference.

It can be seen that results from both models closely match at transient (around 2 s) and in steady state. The EMT's fundamental component is obtained through an FFT block; therefore, a small variation can be observed during the transient.

Figure 6.9 shows the comparison of waveforms between the complete EMT model and the dynamic phasor model with inclusion of the harmonics to the same step change in the voltage reference.

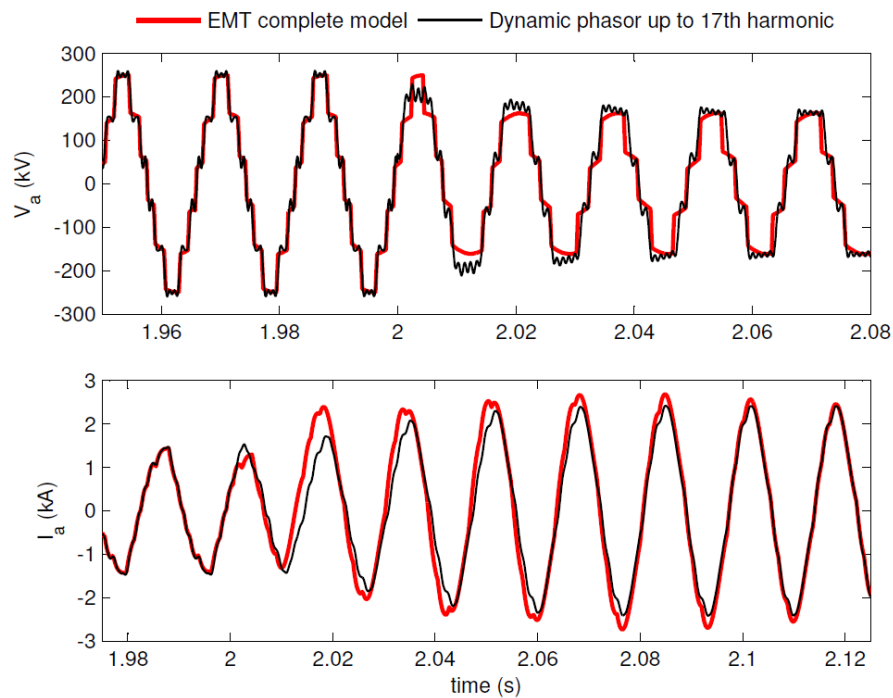


Figure 6.9: Comparison of voltage (top) and current (bottom) with harmonics to a step change in the voltage reference.

From Figure 6.9, it can be observed that the line current increases to maintain constant power flow at 500 MW for the terminal voltage reduction from 1 p.u to 0.75 p.u. Also in the dynamic phasor model the level change from 6 to 4 in voltage waveform can

be clearly observed. The harmonic content of the voltage at 1.0 p.u. and 0.75 p.u. are shown in Figure 6.10.

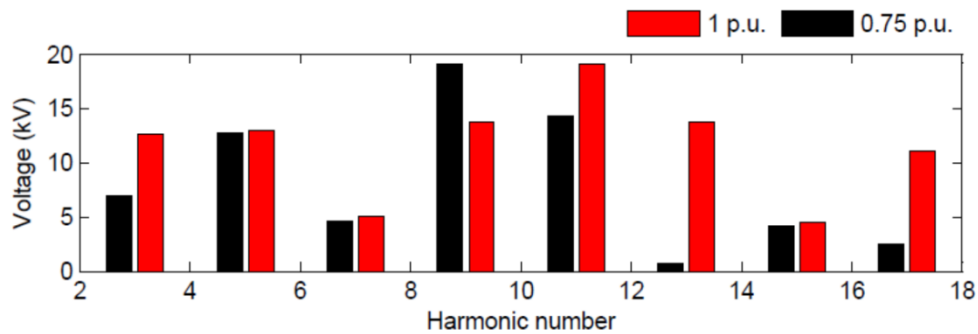


Figure 6.10: Harmonic variation for the step change in terminal voltage.

It can be observed from Figure 6.10 that the dominant harmonic (after fundamental) changes from 11th to 9th when the RMS voltage is changed from 1 p.u. to 0.75 p.u. The reason for the above change is that the number of levels in the output voltage decreased from 6 to 4 as in Figure 6.9.

6.3.3 Results with a step change in power order

A step change to the real power order from 300 MW to 500 MW is applied to both models at 2 s and the RMS power variation obtained from the dynamic phasor model is shown in Figure 6.11.

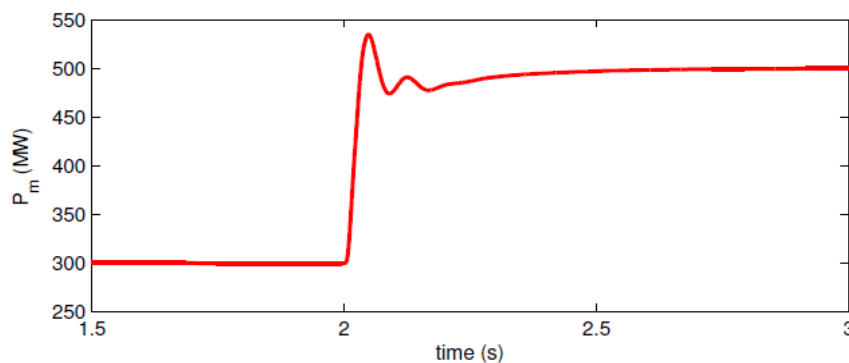


Figure 6.11: Response to a step change in terminal real power.

Figure 6.12 shows the variation in the phase ‘a’ voltage and current (fundamental component only) waveforms in response to the power order change.

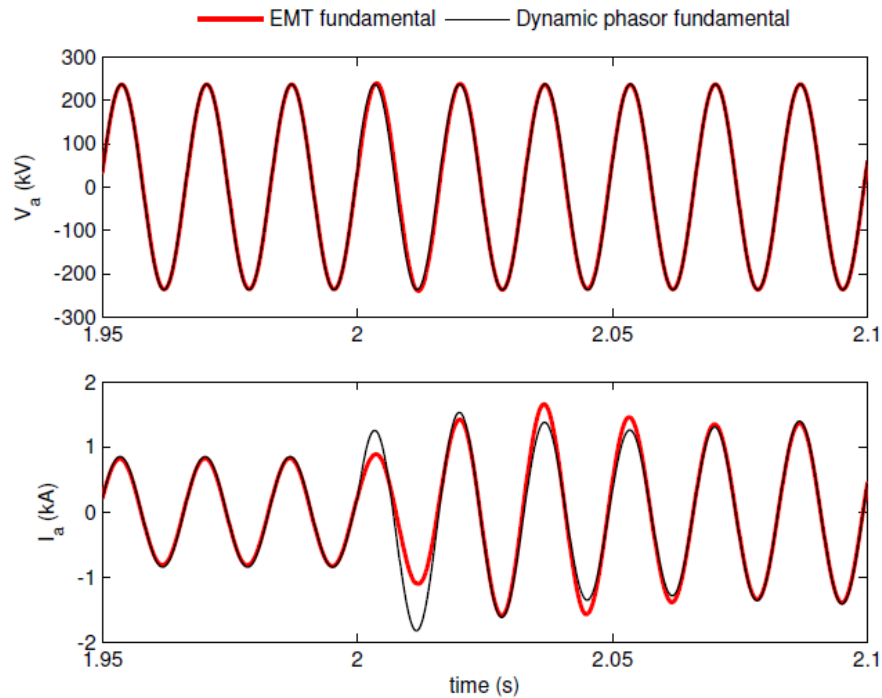


Figure 6.12: Comparison of voltage (top) and current (bottom) fundamental only to a step change in the power reference.

It is observed that the dynamic phasor model closely follows the step change compared to the EMT model. It must be noted that similar to the previous case, the fundamental component of the EMT solution is obtained using a standard FFT block in PSCAD/EMTDC from the originally simulated waveform that included all harmonics. Therefore, a small variation can be observed during the transient.

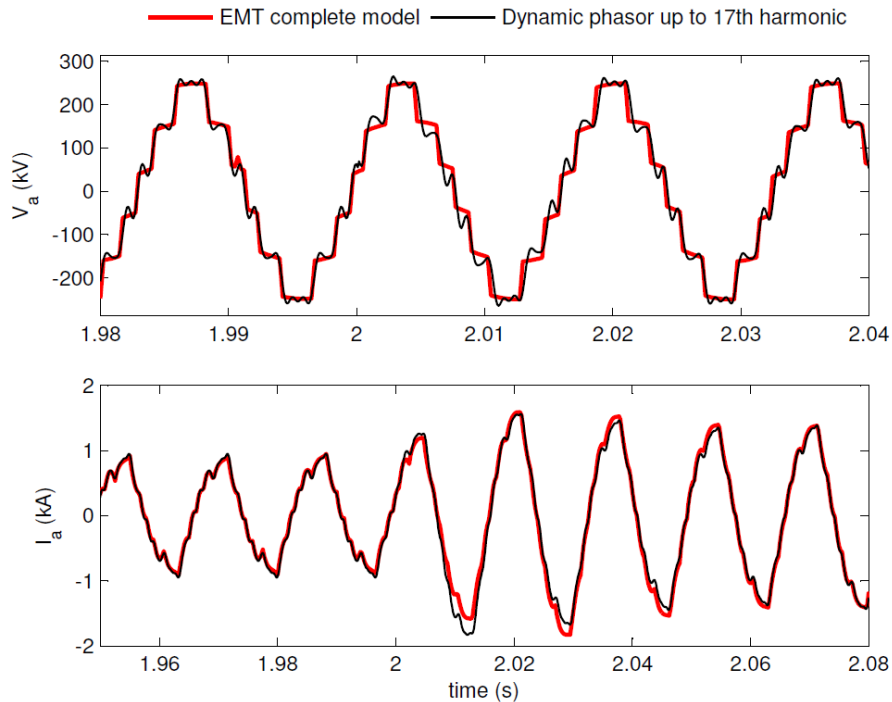


Figure 6.13: Comparison of voltage (top) and current (bottom) with harmonics to a step change in the power reference.

Figure 6.13 shows the phase 'a' voltage and current with inclusion of harmonics for a step change in the power order. It can be observed that the power order change does not affect the ac voltage in a noticeable way and the change is only observed in the line current. Therefore, there is no change in harmonic values since there is no change in voltage reference.

6.4 Analysis on the accuracy of the model

It is straightforward to note that a dynamic phasor based model can be made more accurate if a larger number of harmonics are included in the model. This section shows how doing so affects the accuracy of a simulated waveform. As an example, the dynamic

phasor-based representation of the terminal voltage waveform with an increasing number of odd harmonic is compared against the actual staircase waveform. The period of the waveform in steady state is considered to calculate the RMS voltage error as shown in Figure 6.14. The magnitude difference in RMS voltages from both EMT model and dynamic phasor model is defined as the error. The RMS error between the voltages is calculated as below.

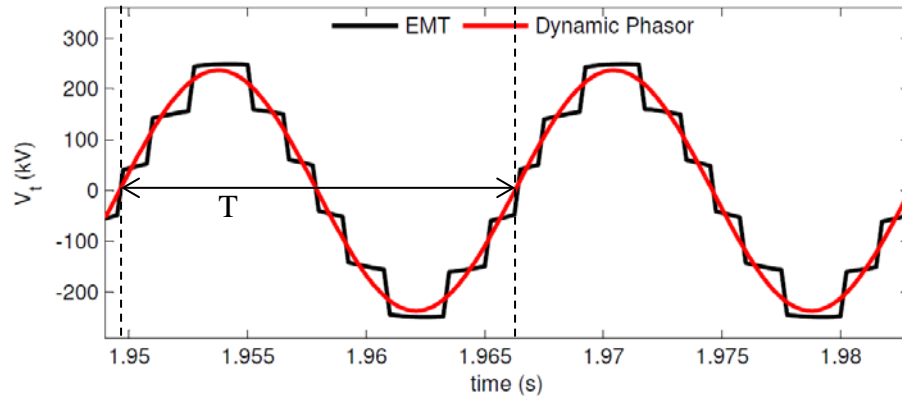


Figure 6.14: Comparison between voltage waveforms of EMT and dynamic phasor model

$$V_{error}(t) = V_{EMT}(t) - V_{DP}(t) \quad (6.1)$$

$$V_{RMS-error} = \frac{\sqrt{\frac{1}{T} \int (V_{error}(t))^2}}{|V_{fundamental}|} \quad (6.2)$$

Table 6.3: RMS voltage error for odd harmonic addition respective to Figure 6.2

Harmonic order	1 st	3 rd	5 th	7 th	9 th	11 th	13 th	15 th	17 th
V_{error} (p.u.)	0.0991	0.0968	0.0958	0.0977	0.0888	0.0908	0.0778	0.0768	0.0752

The RMS voltage error is plotted in Figure 6.15 as a function of the number of harmonic components included.

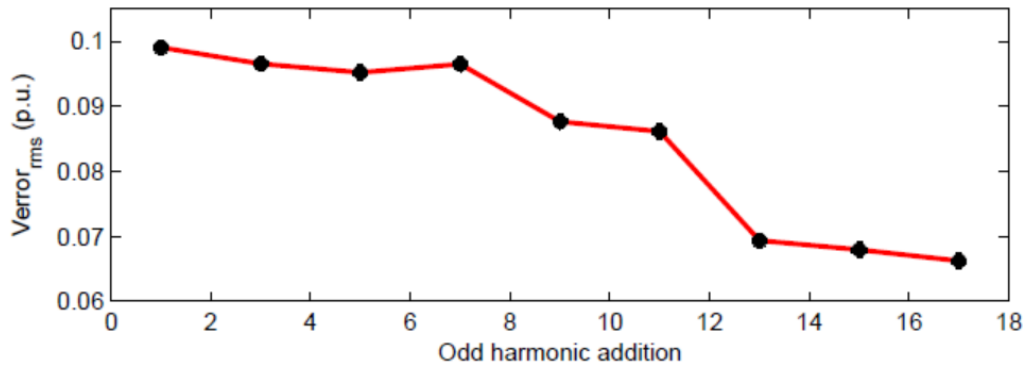


Figure 6.15: Comparison of the model error as a function of harmonics included.

It can be observed from Figure 6.15 that inclusion of every odd harmonic (up to 17th as shown) leads to a reduction in RMS error. It must be noted that in practical MMC configurations, a much larger number of submodules are normally used. Therefore, the harmonic contents of the actual voltage waveform will be much reduced compared to the case considered in this thesis. As such it is expected that for simulations of practical MMC systems, a much smaller number of harmonics needs to be included to achieve high levels of accuracy.

6.5 Summary

In this chapter, a brief introduction of EMT modeling and solving techniques were mentioned. Following that, the MMC model developed in PSCAD/EMTDC tool for dynamic phasor model validation purpose was discussed. The MMC test system parameters used for the simulation were also given.

In the results, the contribution from every odd harmonic to the final staircase voltage waveform was discussed. Furthermore, to test the accuracy of the model, step

disturbances were applied to the reference voltage and simulation results were compared and validated. Also the harmonics' variations for the voltage step change were discussed. Then, a step change was applied to the power reference and the results obtained from both models were compared with inclusion of harmonics. Finally, the reduction in error by adding harmonics was discussed.

Chapter 7

Contributions, Conclusions, and

Future work

7.1 Contributions and conclusions

The following shows the contributions made in this thesis along with conclusions that are drawn from each contribution.

1. An extended-frequency dynamic phasor model of an MMC was developed using dynamic phasor preliminaries.
 - i. This model is general and scalable to accommodate any number of submodules.
 - ii. The harmonics are interrelated to each other. Adding harmonic cause small changes in harmonics that have been already added to the model.
 - iii. For each MMC system, depending on the number of levels, the immediate dominant harmonic after the fundamental is different. For example for a 5-

level MMC, the 11th harmonic is dominant and for a 3-level, the 9th harmonic is dominant, which can be observed by analyzing the Fourier coefficients of the ac voltage waveform.

2. The dynamic phasor model of the direct control system was developed with the help of the phasor model of a PLL [11].
 - i. The direct control method was utilized to control the active power and terminal voltage of an MMC that is connected to an ac system.
 - ii. Real power controller consists of a PI controller and a phase shift value. Therefore, only the products of the fundamental values were considered and the other odd harmonics in current were neglected as they were small in magnitude.
 - iii. Since the harmonics (other than fundamental) in voltage cannot be neglected, separate PI controllers were developed to control each harmonics in voltage control of the dynamic phasor model. Each of these PI controllers output different modulation indices for each odd harmonic to generate switching signals.
3. The developed dynamic phasor model of the MMC was validated against the EMT simulation model with fundamental as well as with inclusion of harmonics.
 - i. It was observed that the fundamental frequency results of the dynamic phasor model closely matched with the fundamental frequency response of the EMT simulation model obtained using the discrete Fourier transformation component available in PSCAD/EMTDC simulation tool.

- ii. In addition, it was shown that by adding more number of harmonics to the dynamic phasor model, further accuracy was achieved.
 - iii. It was shown that a dynamic phasor model, even with consideration of an extended number of harmonics, is executable with a much larger time-step than what is required in an EMT simulation. Therefore, it can be said that the dynamic phasor model offers a significant computational advantage.
 - iv. The error in RMS voltage (magnitude difference between the results from both models) was observed and showed that the addition of harmonics lesser the RMS voltage error.
4. Model validation was done by applying identical disturbances to both dynamic phasor and EMT models and by comparing the time-domain simulation results from both models.
- i. The step change in terminal voltage caused expected changes in voltage levels of the output voltages of the converter and constant real power was achieved.
 - ii. The step change in real power caused changes in current and not in voltage. Therefore, a constant voltage was achieved as expected.
5. The important contributions of this thesis work are published in following scientific publications.
- i. Journal paper
S. Rajesvaran and S. Filizadeh, "Wide-Band Modeling of Modular Multilevel Converters Using Extended-Frequency Dynamic Phasors", (to be published) *Scientia/Iranica*, 2016 (20 pages).

ii. Conference paper

S. Rajesvaran and S. Filizadeh, "Modeling of Modular Multilevel Converter using extended-frequency Dynamic Phasors", in *Proc. IEEE PES Annual General Meeting*, Boston, July 2016 (6 pages).

7.2 Future work

1. In this thesis, a small number of submodules was considered because of the computational limitations associated with the EMT simulation model that was used for validation. Selecting an MMC with large number of submodules and validating with average model of an MMC developed in EMT as mentioned in literature would be a useful extension from a practical viewpoint.
2. Large-valued submodule capacitors were used to reduce the effect of circulating currents. However, the presence of circulating current results in converter losses. Therefore, it would be necessary to include a circulating current suppression controller in the dynamic phasor model.
3. The dynamic phasor model was developed in abc frame. However, developing an MMC model in d-q frame could be useful because the reduction in number of phases can reduce the number of equations and could be simulated with a larger time-step.
4. Although this thesis utilized the direct control for simplicity, the d-q decoupled control is widely used as the control system for MMCs. Therefore, another future

work could be to model the d-q decoupled control with both outer and inner loop controllers and with the inclusion of harmonics.

5. This thesis validated the dynamic phasor model against the EMT simulation model on PSCAD/EMTDC. However, it would be interesting to build a small-scale hardware prototype of the MMC test system and validate the dynamic phasor model.
6. Developing the dynamic phasor model in an EMT platform and simulation time analysis with the actual model developed using EMT simulation tool.

References

- [1]. J. Dorn, H. Huang, D. Retzmann, "A new Multilevel Voltage-Sourced Converter Topology for HVDC Applications," *In CIGRÉ session*, 2008.
- [2]. B. Jacobson, P. Karlsson, G. Asplund, L. Harnefors, and T. Jonsson, "VSC-HVDC transmission with cascaded two-level converters," *B4-110-2010, CIGRE Meeting, Paris, France*, Aug. 2010.
- [3]. A. Nami, J. Liang, F. Dijkhuizen, and G.D. Demetriades, "Modular multilevel converters for HVDC applications: review on converter cells and functionalities," *IEEE Trans. Power Electron.*, vol. 30, no. 1, pp. 18–36, Jan. 2015.
- [4]. D.R. Trainer, C.C. Davidson, C.D.M. Oates, N.M. Macleod, D.R. Critchley, and R.W. Crookes, "A new hybrid voltage-sourced converter for HVDC power transmission," *B4-111-2010, CIGRE Meeting, Paris, France*, Aug. 2010.
- [5]. J. Rodriguez, L. Jih-Sheng, and P. Fang Zheng, "Multilevel inverters: a survey of topologies, controls, and applications," *IEEE Transactions on Industrial Electronics*, vol. 49, pp. 724-738, 2002.
- [6]. S. Debnath, J. Qin, B. Bahrani, M. Saeedifard, and P. Barbosa, "Operation, control, and applications of the modular multilevel converter: A review," *IEEE Trans. Power Electron.*, vol. 30, no. 1, pp. 37–53, Jan. 2015.

- [7]. S. Chiniforoosh, J. Jatskevich, A. Yazdani, V. Sood, V. Dinavahi, J. Martinez, and A. Ramirez, "Definitions and applications of dynamic average models for analysis of power systems," *IEEE Trans. Power Del.*, vol. 25, no. 4, pp. 2655–2669, Oct. 2010.
- [8]. M. M. Z. Moustafa and S. Filizadeh, "A VSC-HVDC model with reduced computational intensity," in *Proc. IEEE Power and Energy Society General Meeting–2012*, pp. 1–6
- [9]. S.R. Sanders, J.M. Noworolski, X.Z. Liu, and G.C. Verghese, "Generalized averaging method for power conversion circuits," *IEEE Trans. Power Electron.*, vol. 6, no. 2, pp. 251–259, Apr. 1991.
- [10]. W. Yao, J. Wen, and S. Cheng, "Modeling and simulation of VSC-HVDC with dynamic phasors," in *Proc. Electric Utility Deregulation and Restructuring and Power Technologies (DRPT 2008)*, pp. 1416–1421, Apr. 2008.
- [11]. M. Daryabak, S. Filizadeh, J. Jatskevich, A. Davoudi, M. Saeedifard, V.K. Sood, J.A. Martinez, D. Aliprantis, J. Cano, and A. Mehrizi-Sani, "Modeling of LCC-HVDC systems using dynamic phasors," *IEEE Trans. on Power Del.*, vol. 29, no. 4, pp. 1989–1998, Aug. 2014.
- [12]. C. Liu, A. Bose, and P. Tian, "Modeling and analysis of HVDC converter by three-phase dynamic phasor," *Power Delivery, IEEE Transactions on*, vol. 29, no. 1, pp. 3–12, Feb 2014.
- [13]. S. Chandrasekar, R. Gokaraju, "Dynamic phasor modeling of type 3 DFIG wind generators (including SSCI phenomenon) for short-circuit calculations," in *IEEE Trans. on Power Del.*, vol. 30, no. 2, pp. 887–897, April 2015.

- [14]. T. Yang, S. Bozhko, Jean-Mark Le-Peuvedic, G. Asher, and Christopher Ian Hill "Dynamic Phasor Modeling of Multi-Generator Variable Frequency Electrical Power Systems," in *IEEE Trans. on Power sys.*, vol. 31, no. 1, pp. 563–571, Jan 2016.
- [15]. S.R. Deore, P.B. Darji, and A.M. Kulkarni, "Dynamic phasor modeling of modular multi-level converters," in *Proc. IEEE International Conference on Ind. and Inf. Sys. (ICIIS)*, pp.1–6, Aug. 2012.
- [16]. P. B. Darji and A. M. Kulkarni, "Dynamic performance of a modular multi-level converter based HVDC terminal under unbalanced AC grid conditions," in *Proc. 10th Int. Conf. AC-DC Power Transmiss.*, 2012, pp. 1–6.
- [17]. D. Jovcic, A. Jamshidifar, "Phasor model of modular multilevel converter with circulating current suppression control," in *IEEE Trans. on Power Del.*, vol. 30, no. 4, pp. 1889-1897, Aug. 2015.
- [18]. S. Filizadeh, "ECE 7072 – Advanced power electronics," *Course notes, Dept. Elec. and Comp. Eng., University of Manitoba*. Jan. 2014.
- [19]. N. Mohan, T. M. Undeland, W. P. Robbins, "Power electronics: converters, applications and design," *third ed., John Wiley & Sons, Inc.*, 2003.
- [20]. Q. Tu, Z. Xu, and L. Xu, "Reduced switching-frequency modulation and circulating current suppression for modular multilevel converters," *IEEE Trans. Power Del.*, vol. 26, no. 3, pp. 2009–2017, Jul. 2011.
- [21]. M. Saeedifard and R. Iravani, "Dynamic performance of a modular multilevel back-to-back HVDC system," *IEEE Trans. Power Del.*, vol. 25, no. 4, pp. 2903–2912, Oct. 2010.

- [22]. A. Gole, "ECE 7440 – VSC HVDC Integration" *Course notes, Dept. Elec. and Comp. Eng., University of Manitoba*. Jan. 2014.
- [23]. H. Ghoreishy, A. Y. Varjani, M. Mohamadian, S. Farhangi, and Z. Zhe, "A new selective harmonic elimination pulse-width and amplitude modulation (SHE-PWAM) for drive applications," in *Proc. 39th Annu. IEEE IECON/IECON*, 2013, pp. 234–239.
- [24]. G. Konstantinou, M. Ciobotaru, and V. Agelidis, "Selective harmonic elimination pulse-width modulation of modular multilevel converters," *IET Power Electron.*, vol. 6, no. 1, pp. 96–107, Jan. 2013.
- [25]. A. Kiani Harchegani and H. Iman-Eini, "Selective harmonic elimination pulse width modulation in single-phase modular multilevel converter," *Power Electronics, Drives Systems & Technologies Conference (PEDSTC), 2015 6th*, Tehran, 2015, pp. 346-351.
- [26]. Y. Deng, M. Saeedifard, and R. G. Harley, "An optimized control strategy for the modular multilevel converter based on space vector modulation," in *Proc. IEEE Appl. Power Electron. Conf. Expo.*, Mar. 2015, pp. 1564–1569.
- [27]. Y. Deng and R. G. Harley, "Space-vector versus nearest-level pulse width modulation for multilevel converters," *IEEE Trans. Power Electron.*, vol. 30, no. 6, pp. 2962–2974, Jun. 2015.
- [28]. Y. Deng, Y. Wang, K. H. Teo and R. G. Harley, "A Simplified Space Vector Modulation Scheme for Multilevel Converters," in *IEEE Transactions on Power Electronics*, vol. 31, no. 3, pp. 1873-1886, March 2016.

- [29]. M. Saeedifard, H. Nikkhajoei, R. Iravani, and A. Bakhshai, "A space vector modulation approach for a multi module HVDC converter system," *IEEE Trans. Power Del.*, vol. 22, no. 3, pp. 1643–1654, Jul. 2007.
- [30]. P.M. Meshram and V.B. Borghate, "A simplified nearest level control (NLC) voltage balancing method for modular multilevel converter (MMC)," *IEEE Trans. on Power Electron.*, vol. 30, no. 1, pp. 450–462, Jan. 2015.
- [31]. C. Schauder and H. Mehta, "Vector analysis and control of advanced static var compensators," in *Conference Publication no. 345 of the IEE Fifth International Conference on AC and DC Power Transmission*, London, September 1991, pp. 266-272.
- [32]. I. Papic, P. Zunko, and D. Povh, "Basic control of unified power flow controller," *IEEE Trans. Power Syst.*, vol. 12, no. 4, pp. 1734–1739, Nov. 1997.
- [33]. R. M. Santos Filho, P. F. Seixas, P. C. Cortizo, L. A. B. Torres, and A. F. Souza, "Comparison of three single-phase PLL algorithms for UPS applications," *IEEE Trans. Ind. Electron.*, vol. 55, no. 8, pp. 2923–2932, Aug. 2008.
- [34]. V. A. Caliskan, O. C. Verghese, and A.M. Stankovic, "Multifrequency averaging of dc-dc converters," *IEEE Trans. Power Electron.*, vol. 14, no. 1, pp. 124–133, Jan. 1999.
- [35]. P. Mattavelli, G. C. e. Verghese, and A. M. Stankovic, "Phasor dynamics of thyristor-controlled series capacitor systems," *IEEE Trans. Power Syst.*, vol. 12, no. 3, pp. 1259–1267, Aug. 1997.

- [36]. P. C. Stefanov and A. M. Stankovic, "Modeling of UPFC operation under unbalanced conditions with dynamic phasors," *IEEE Trans. Power Syst.*, vol. 17, no. 2, pp. 395–403, May 2002.
- [37]. A. M. Stankovic and T. Aydin, "Analysis of asymmetrical faults in power systems using dynamic phasors," *IEEE Trans. Power Syst.*, vol. 15, no. 3, pp. 1062–1068, Aug. 2000.
- [38]. T. H. Demiray, "Simulation of power system dynamics using dynamic phasor models," *Ph.D. dissertation, Dept. Elect. Eng., Swiss Fed. Inst. Technol., Zurich, Switzerland*, 2008.
- [39]. M. A. Kulasza "Generalized Dynamic Phasor-Based Simulation for Power Systems," *M.Sc. dissertation, Dept. Elect. and Comp. Eng., University of Manitoba, Canada*, 2014.
- [40]. A. Gole, "ECE 7310 – Transient simulation" *Course notes, Dept. Elec. and Comp. Eng., University of Manitoba*. Jan. 2015.
- [41]. M. M. Z. Moustafa, "Operating Limits and Dynamic Average-Value Modelling of VSC-HVDC Systems," *Ph.D. dissertation, Dept. Elect. and Comp. Eng., University of Manitoba, Canada*, 2011.
- [42]. U. Gnanarathna, A. Gole, and R. Jayasinghe, "Efficient modeling of modular multilevel hvdc converters (MMC) on electromagnetic transient simulation programs," *IEEE Trans Power Del.*, vol. 26, no. 1, pp. 316–324, Jan. 2011.
- [43]. H. Saad, S. Denetiere, J. Mahseredjian, P. Delarue, X. Guillaud, J. Peralta, and S. Nguefeu, "Modular multilevel converter models for electromagnetic transients," *IEEE Trans. Power Del.*, vol. 29, no. 3, pp. 1481–1489, Jul. 2014.

- [44]. Manitoba HVDC Research Center, *EMTDC User's Guide*, Winnipeg, MB, Canada, 2003.